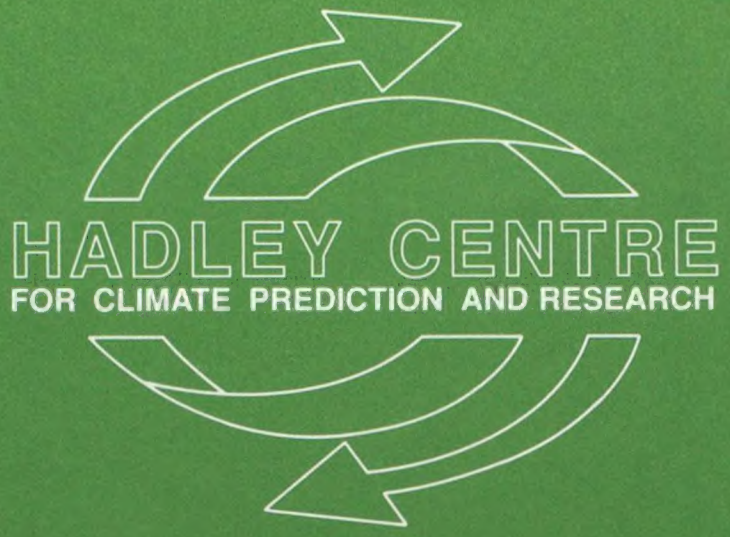

Seasonal uptake of anthropogenic CO_2 in an ocean general circulation model

by

N K Taylor

CRTN 47

May 1994

CLIMATE
RESEARCH
TECHNICAL
NOTE

Hadley Centre
Meteorological Office
London Road
Bracknell
Berkshire RG12 2SY

CLIMATE RESEARCH TECHNICAL NOTE NO. 47

SEASONAL UPTAKE OF ANTHROPOGENIC CO_2 IN AN OCEAN GENERAL CIRCULATION MODEL

by

N K Taylor

May 1994

Hadley Centre for Climate Prediction and Research
Meteorological Office
London Road
Bracknell
Berkshire RG12 2SY

NOTE: This paper has not been published. Permission to quote from it should be obtained from the Director of the Hadley Centre.

SEASONAL UPTAKE OF ANTHROPOGENIC CO_2 IN AN OCEAN GENERAL CIRCULATION MODEL

Nicholas K. Taylor
Hadley Centre for Climate Prediction and Research
Meteorological Office
London Road
Bracknell
UK

ABSTRACT

A model of the inorganic carbon cycle, embedded within an ocean general circulation model is described, and results from a seasonal simulation of the present-day ocean carbon cycle are presented. Whilst the circulation characteristics of the model appear reasonable, the model gives North Atlantic Deep Water rates that are too low compared with deep water of southern origin, which may result in an overestimate of the southern hemisphere uptake. A comparison of the model results with available observations of dissolved inorganic carbon and partial pressure of carbon dioxide reveals that a defect in the present model is the neglect of ocean biology, which causes the phase of seasonal variations in partial pressure in high latitudes to be incorrectly simulated. A series of experiments were performed in which CO_2 was added to the atmosphere at a specific rate to simulate anthropogenic emissions. The model predicts an oceanic uptake of 44% of atmospheric emissions at the end of a 50 year run. The largest sinks in the model occur in the southern hemisphere and equatorial regions. A comparison between parallel runs made under conditions of seasonally varying and annual-mean forcing reveals that the use of seasonal forcing in the present model makes little difference to the estimate of global oceanic uptake of anthropogenic CO_2. Varying the background coefficient of vertical diffusion, within commonly accepted limits, is found to have a much greater impact on CO_2 uptake estimates.

1 INTRODUCTION

In recent years there has been a great deal of interest in the role of the so-called greenhouse gases in climate and the possibility of climate change brought about by man's activities in significantly increasing their atmospheric concentration. A related area that has also attracted a lot of attention is that of the carbon cycle. The reason for this is that since CO_2 is the dominant greenhouse gas, the past, present and future movements of carbon between its various source and sinks needs to be known in some detail if we are to understand present-day and past levels of greenhouse gas concentrations in the atmosphere and if we are to be able to predict the course of climate change into the future.

Predictions of future climate made using global climate models (GCMs) depend upon knowing what the future amount of CO_2 and other trace gases will be in the atmosphere. At present, these models are either run in "equilibrium mode" whereby the model's equilibrium climate is determined for set levels of atmospheric concentration of CO_2 (such as double the present-day amount), or they are run in "transient mode" where the CO_2 in the atmosphere is assumed to increase at a prescribed, usually ad hoc, rate such as a 1% compound increase per year. Alternatively, transient CO_2 experiments may be run using a prescribed increase in atmospheric CO_2 which is derived from estimates of future emissions of fossil fuel combined with estimates of how much anthropogenic carbon remains in the atmosphere. These estimates stem from rather simple box models which do not fully capture the three-dimensonal complexity of the real world. Furthermore, the box models assume that in the future the carbon cycle will operate in exactly the same manner as it does at present. In a world in which global warming is taking place this assumption is not necessarily correct. There are numerous feedbacks, both positive and negative, between the climate and carbon cycle systems which could cause the carbon cycle to act in a fundamentally different manner than at present. For instance, increases in surface heating and precipitation at high latitudes may cause increased density stratification of the ocean, leading to a reduction in the rate of deep water formation and a smaller flux of CO_2 from the atmosphere into the oceans in these regions. Alternatively, changes in wind forcing which cause an increase in the supply of nutrients to surface waters could lead to increased growth of phytoplankton and an increased flux of carbon from the surface ocean to the deep sea, resulting in a larger invasion of atmospheric CO_2 into the ocean. For these reasons, when attempting to make predictions of future climate using coupled ocean-atmosphere GCMs it is desirable to have a model which is able to take account of these feedbacks and which can compute the concentration of CO_2 in the atmosphere as a response to climate change.

Another reason for having such a model is that remarkably little is understood about the workings of today's global carbon cycle system. Until recently it was estimated on the basis of simple box models that the net flux into the oceans was 2.0±0.8 GtC yr^{-1} (IPCC, 1990). Tans *et al* (1990) challenged this estimate on the basis that the interhemispheric transport in their 3-D atmospheric model was insufficient to allow a sizeable southern hemisphere sink for anthropogenic CO_2 produced in the northern hemisphere, whilst an analysis of observed differences between atmospheric and oceanic partial pressures could account for a net northern hemisphere uptake of at most 1.0 GtC yr^{-1}. Since then, Sarmiento *et al* (1992) have published results from a 3-D ocean model which agree with the IPCC figure and attempts have been made to reconcile their estimate with the Tans *et al* (1990) result by consideration of, amongst other things, the transport of carbon into the ocean by rivers (Sarmiento and Sundquist, 1992), the thermal skin effect in calculating pCO_2 (Robertson and Watson, 1992), the effect of ocean biota in producing variations in pCO_2 (Watson *et al* 1991), and the effect of a large southern hemisphere source and northern hemisphere sink in pre-industrial times linked with a southward transport of carbon in the pre-industrial ocean (Broecker and Peng, 1992). Further uncertainties remain, such as the role of the coastal zones and burial in sediments. There is a need for more and better estimates of the sink strength of the ocean for anthropogenic CO_2. More accurate esimates of the role of the ocean as a sink for atmospheric CO_2 will serve to constrain the net effect of the terrestrial biosphere which is even more difficult to quantify than the ocean.

The Sarmiento *et al* (1992) results were obtained using the Geophysical Fluid Dynamics Laboratory (GFDL) ocean model, and did not include a seasonal cycle. Apart from the Sarmiento *et al* (1992) study, the only other 3-D simulations of the ocean carbon cycle have been those produced by Maier-Reimer and Hasselmann (1987) and Bacastow and Maier-Reimer (1990) using the Hamburg large-scale geostrophic GCM. The former study uses annual-mean forcing whilst the latter includes a seasonal cycle and a parametrization of the biological particle flux into the deep ocean. In these models atmospheric CO_2 forcing is provided by a time-series of the historical fossil fuel production, whilst the Sarmiento *et al* (1992) model is forced by an imposed atmospheric CO_2 concentration history. Both the GFDL and Hamburg models have a relatively coarse resolution (5°x5°, 10 layers for the Hamburg model; 3.75°x4.5°, 12 layers for the GFDL model). Sarmiento *et al* (1992) found that the Hamburg model took up approximately 12% more CO_2 than the GFDL model.

This paper describes integrations made with a global carbon cycle model coupled to a 3-dimensional ocean general circulation model. The model used can be run coupled to an atmospheric GCM for investigation of feedbacks from the carbon cycle to the climate system, although in the present study we use prescribed climatological atmospheric forcing. The model described here includes only the physical and chemical mechanisms

of carbon uptake operating on timescales up to a thousand years. No attempt is made to model the effect of ocean biology on the uptake of atmospheric carbon, nor do we consider the terrestrial carbon cycle, or processes thought to be important on geological timescales. The neglect of biology can be justified on the grounds that we are mainly interested in the uptake of anthropogenic CO_2, which involves looking at the difference between simulations with and without additional CO_2 added to the atmosphere. The effect of biology is assumed to be the same in both cases. This is a reasonable assumption if biological productivity is limited by lack of nutrients over much of the ocean so that the biological pump will be essentially unaffected by increased atmospheric CO_2 levels. This assumption is not necessarily correct, however, as it neglects the role of feedbacks between the biological pump and the climate system, but is nevertheless a useful starting point. The effect of terrestrial biota as a net source or sink of CO_2 is a moot point. Keeling and Shertz (1992) have sought to place constraints on its role by measuring oxygen to nitrogen ratios, and conclude that the effect of deforestation is roughly compensated by the carbon fertilisation effect, although the errors involved in this calculation are as yet very large. Future versions of the model will simulate nutrient, phytoplankton and zooplankton concentrations and their effect on the flux of carbon between surface and intermediate and deep waters. A model of the land carbon cycle is also under development. The present model will serve as a useful yardstick against which later models can be compared.

A more serious omission is the neglect of important feedback mechanisms in the model. The experiment described below in which anthropogenic CO_2 is added to the atmosphere assumes that the ocean is forced in exactly the same way with extra CO_2 as it was before the CO_2 was added. In other words, we ignore the effect that any climate change might have on the operation of the carbon cycle. There are a number of potential feedbacks between the carbon cycle and climate change/global warming, involving, amongst other things, increased sea surface temperature and hence increased pCO_2, changes in the rate of deep water formation, changes in surface fluxes due to changed wind patterns as well as the biological feedbacks just mentioned. Taylor (1992) gives a more complete list of possible feedbacks. The proper investigation of these mechanisms would require the carbon cycle model to be incorporated into a coupled atmosphere-ocean model, the development of which is one of the ultimate aims of this work.

In this study we take a somewhat different approach to that used by the GFDL and Hamburg groups. Instead of simulating a particular historical period, we ask the following question: what proportion of a given amount of fossil fuel emitted to the atmosphere is the ocean capable of absorbing over a timescale of 50 years? To answer this, we spin up a coupled ocean-carbon cycle model until it is in equilibrium with an imposed atmospheric concentration of 348 ppm. We then proceed to add CO_2 to the atmosphere at a constant rate and observe

the uptake of this additional CO_2 by the ocean. Both seasonal and annual-mean simulations are performed and the results compared. Finally, we look at the effect of changing the vertical diffusion characteristics of the model on uptake of CO_2. The approach adopted, whilst appropriate for studying the response of the model to an atmospheric CO_2 perturbation, is somewhat non-standard and this makes comparison with other models difficult. We are also carrying out a series of simulations under more conventional forcing conditions for the purpose of model intercomparison, and these will be published separately.

The model is described in section 2. Section 3 describes the model spin-up. The behaviour of the circulation model is discussed in section 4.1. Section 4.2 describes the carbon cycle results under seasonal forcing conditions, and presents results from a seasonal integration in which the uptake of anthropogenic CO_2 by the ocean is calculated. These results are compared with results from a similar run using annual mean forcing in section 4.3, and in section 4.4 we also look at the sensitivity of the modelled uptake to the coefficient of vertical diffusion, a poorly-known parameter. Results are summarised in section 5.

2 MODEL DESCRIPTION

2.1 Ocean Circulation Model

The ocean circulation model used is based upon the 3-D primitive equation model described by Bryan (1969) and Cox (1984), which solves the Navier-Stokes equations modified by the Boussinesq approximation and hydrostatic assumption. Prognostic variables are temperature, salinity, and zonal and meridional velocity. Density is computed from temperature and salinity using a polynomial approximation to the equation of state for seawater (Bryan and Cox, 1972) and vertical velocity is diagnosed from the continuity equation. A detailed description of the equations and their method of solution can be found in the above references. The model employed here is global and includes a realistic approximation to bottom topography and continental coastlines. A horizontal grid resolution of 2.5° latitude by 3.75° longitude was chosen to match the resolution of the Hadley Centre atmospheric climate model (Murphy, 1994). 20 levels are used in the vertical with 7 levels covering the top 113 metres (Table 1). The near-surface resolution is somewhat higher than other models of this type, since it is recognized that a good representation of vertical mixing processes near to the surface is important for modelling the seasonal exchange of CO_2 with the atmosphere. A Kraus-Turner type bulk mixed

layer model (Kraus and Turner, 1967) is incorporated within the ocean model in order to improve the simulation of the seasonal cycle of sea surface temperature and mixed layer depths. In the present version of the model, SST is not permitted to drift far away from observations (see below), but future versions will be coupled to an atmospheric GCM, and it will then become important to reduce errors in simulating seasonal changes in SST. Energy provided by wind mixing power is used to mix the surface heat and freshwater input throughout the mixed layer. Wind-mixing energy is decayed exponentially with depth to prevent over-deepening of the winter-time mixed layer. Convection in the mixed layer is partly penetrative in that 85% of convectively generated turbulent kinetic energy is dissipated within the mixed layer. Penetrative short wave radiation is represented by a double exponential decay function (Paulson and Simpson, 1977). As well as the Kraus-Turner scheme, we use the K-theory mixing scheme of Pacanowski and Philander (1981) to parametrize Richardson-Number-dependent vertical turbulent mixing in which K_m, K_h are given by

$$K_m = \upsilon_0 / (1+\alpha Ri)^n + \upsilon_b \qquad (1)$$

$$K_h = K_m / (1+\alpha Ri) + \chi_b \qquad (2)$$

Ri is the Richardson number,

$$Ri = (-g/\rho\ \partial\rho/\partial z) / |\partial u/\partial z|^2 \qquad (3)$$

υ_b and χ_b are minimum background values of the eddy viscosity and diffusivity, chosen as 0.1 cm^2s^{-1} and 0.5 cm^2s^{-1} respectively, and υ_0 , α and n are adjustable parameters whose values were taken from Pacanowski and Philander's paper (where they were chosen to fit the observed strength of the equatorial undercurrent). Below the thermocline the values used by the model are essentially the background ones. The background vertical mixing coefficient for tracers lies towards the middle of the range of values typically used (0.1 to 1.3 $cm^2\ s^{-1}$), and was chosen in order to avoid numerical problems which can occur when a non-uniform vertical grid is used. Yin and Fung (1991) have shown that a negative effective vertical diffusivity may be produced in regions of strong downwelling when a low value of diffusivity is combined with variable grid spacing, such as that used here. One way around the problem is to increase the explicit vertical diffusivity, which is the approach taken in this study. We also performed one integration using a smaller value of the diffusion coefficient, 0.1 $cm^2\ s^{-1}$ in order to assess the sensitivity of the results to vertical diffusion.

Below the mixed layer a simple parametrization of convective adjustment is used. Pairs of adjacent layers are tested for static instability and are mixed if found to be unstable. The density of the bottom-most layer of one pair is then compared with the top-most layer of the next pair and the layers are mixed again if necessary. This process is repeated several times to ensure stability.

A parametrization of isopycnal diffusion (Redi, 1982 ; Cox, 1987) is included so that the dominant direction of mixing for tracers such as heat, salt and carbon lies along surfaces of constant density rather than the horizontal. It is believed that this more accurately mimics the thermocline ventilation and mixing processes that occur in the real ocean. England (1993) found that the inclusion of an isopycnal mixing scheme resulted in an improvement in the simulated production of intermediate water. As in Bryan and Lewis (1979), the isopycnal diffusivity for tracers is assumed to be greater in the upper ocean than in the deep ocean:

$$A_h = A_b + (A_s - A_b) \exp(-z/500) \quad (4)$$

where A_s is the surface value, A_b is the deep ocean value, and z is the depth in metres. In addition to the isopycnal component of diffusivity, a small background horizontal coefficient is included to maintain numerical stability.

Because of the convergence of meridians at high latitudes, horizontal viscosity is decreased away from the equator according to:

$$A_m = A_{m1} + A_{m2} \cos \phi \quad (5)$$

where ϕ is latitude. The smaller coefficient of viscosity at the poles enables a longer timestep to be used without violating the grid cell Reynolds number stability criterion.

The selection of appropriate values for the sub-grid scale mixing parameters can be troublesome since these are not well known. The vertical diffusivity of heat, salt and tracers in particular is problematical because the Bryan-Cox model's thermohaline circulation has been shown to be particularly sensitive to the value chosen (Bryan, 1987). Furthermore, Gargett and Holloway (1992) have shown that the model is also sensitive to the relative magnitudes of the diffusion coefficients for heat and salt when separate coefficients are used. A full list of parameters used within the model is given in Table 2.

The coarse horizontal resolution means that the Straits of Gibraltar are not resolved by the model grid. However, the Mediterranean Sea is included in the model, and exchange through the straits of Gibraltar is parametrized in a very simple way, using the method described by Manabe and Stouffer (1988). At each timestep the tracer properties of the Atlantic and Mediterranean grid points immediately adjacent to the Straits are fully mixed down to a depth of 1200 metres. In this way a source of Mediterranean water is introduced into the Atlantic at the correct depth.

A further addition to the basic Cox (1984) model is the inclusion of a sea-ice model. This is based on the

zero-layer thermodynamic model of Semtner (1976) with a parametrization of leads and polynyas following Hibler (1979). The prognostic variables are ice surface temperature, ice depth, ice concentration, and snow depth. There is no representation of ice dynamics, and hence the wind-stress is passed directly to the ocean beneath the ice. However, atmospheric heat and fresh water fluxes are treated separately over the portions of a grid box covered by ice and by leads. Beneath the ice, the heat flux from the ocean to the ice is assumed to be related linearly to the temperature difference between the top layer of the ocean and the base of the ice. The temperature of the base of the ice is assigned a fixed value of -1.8 °C, the freezing point of water at 35 psu. When sea water freezes, salt is rejected in proportion to the difference between the salinity of the water and that of ice and is used to increase the salinity or the surface water. The salinity of ice is assumed to be constant at 6 psu. When ice melts, the relatively fresh melt-water reduces the salinity of the surface layer. The inclusion of the brine rejection process should give improved deep water formation rates in seasonal simulations. Roberts and Cattle (1989) discuss the performance of the sea-ice model.

The model is forced with Esbensen and Kushnir (1981) heat fluxes and the climatological wind stresses of Hellerman and Rosenstein (1983). Surface fresh water fluxes were obtained by combining the Jaeger (1976) precipitation dataset with evaporation derived from the Esbensen and Kushnir (1981) fluxes. In addition to the prescribed heat and salt fluxes, surface values of temperature and salinity are relaxed back towards climatological values using a method equivalent to that of Haney (1971), so that the surface boundary condition takes the form

$$Q(T) = Q(T_c) + \lambda (T - T_c) \qquad (6)$$

$$F(S) = F(S_c) + \lambda (S - S_c)/C_p \qquad (7)$$

where $Q(T_c)$, $F(S_c)$ are the climatological heat and salt fluxes for the climatological sea surface temperature (T_c) and sea surface salinity (S_c), and T,S are the surface values of temperature and salinity predicted by the model. T_c are derived from a joint UKMO/Massachussets Institute of Technology dataset of SST (Bottomley *et al*, 1990), and S_c are taken from Levitus (1982). C_p is the specific heat capacity of seawater in $J\,Kg^{-1}\,K^{-1}$. λ takes the value $40.9\ Wm^{-2}\,K^{-1}$, which corresponds to a relaxation timescale of about 60 days for a surface mixed layer of depth 50m. This formulation prevents the surface temperatures and salinities from drifting far away from climatology. Sea-ice depths and concentrations are similarly forced back towards a model-derived climatology to prevent excessive drift.

2.2 Carbon Cycle Model

The present version of the carbon cycle model is designed to be as simple as possible. The 3-dimensional distribution of dissolved inorganic carbon is calculated within the interior of the ocean model using

$$\partial C/\partial t + \underline{u} \bullet \nabla C + w\, \partial C/\partial z = A_h \nabla^2 C + \partial(K_h\, \partial C/\partial z) / \partial z \qquad (8)$$

where C is the concentration of dissolved inorganic carbon, also known as TCO2. Except for at the surface, TCO2 is thus treated as an additional conservative tracer by the ocean circulation model. The same mixing coefficients are used for TCO2 as for temperature and salinity. Equation (8) is solved by an on-line, prognostic method. That is, TCO2 is updated at the same time as new velocity, temperature and salinity fields are calculated. An off-line approach to the solution of equation (8) would be computationally cheaper, but would not be suitable for coupling to an atmospheric model, and would introduce errors owing to the intermittency of convection. Sarmiento *et al* (1992) found that an off-line version of their model took up about 10% more carbon than the on-line version.

TCO2 is comprised of three components, whose relative abundance is described by the following chemical equilibrium relations:

$$[H_2CO_3] = k_0\, pCO_2^{(oc)} \qquad (9)$$

$$[H^+][HCO_3^-] = k_1\, [H_2CO_3] \qquad (10)$$

$$[H^+][CO_3^{2-}] = k_2\, [HCO_3^-] \qquad (11)$$

where [ ] denotes concentration. H_2CO_3 is carbonic acid and dissolved gaseous CO_2, CO_3^{2-} is the carbonate ion and HCO_3^- is the bicarbonate ion. $pCO_2^{(oc)}$ is the partial pressure exerted by gaseous CO_2 in parts per million by volume (ppm). k_0,k_1 and k_2 are apparent equilibrium constants, which depend on temperature and salinity. The equations given by Peng *et al* (1987) are used to calculate the equilibrium constants, and the computational procedure of Bacastow (1981) is then used to compute $pCO_2^{(oc)}$ using k_0, k_1, k_2, TCO2 and alkalinity. The Peng *et al* (1987) equations use dissociation constants determined by Mehrbach *et al* (1973). These have been superceded by the more recent measurements of Goyet and Poisson (1989), which are thought to be more accurate. For the purposes of this paper, the differences are very small. Apart from carbonate and bicarbonate ions, borate contributes about 5% to alkalinity and so a correction for borate ion concentration is applied. The variable degree of dissociation of the borate system is also accounted for. Alkalinity is not treated as an additional tracer in this model, since the exclusion of biology means that the processes which can modify it, such as photosynthesis and the removal of calcium carbonate to form shells, are not included in the simulations described here. Exchange of CO_2 with the atmosphere does not alter the sea surface alkalinity because CO_2 is

uncharged. A constant value of alkalinity of 2300 μeq kg^{-1} is used, corresponding to an average salinity of 35 psu.

The flux of carbon dioxide between atmosphere and ocean is expressed as the product of a gas transfer coefficient and the partial pressure difference between air and water (Etcheto and Merlivat, 1988; Tans *et al*, 1990; Thomas *et al*, 1988):

$$\text{Flux} = V_p\, k_0\, (pCO_2^{(atm)} - pCO_2^{(oc)})$$
$$= V_p\, k_0\, \Delta\, pCO_2 \qquad (12)$$

where k_0 is the CO_2 solubility given above, $pCO_2^{(atm)}$ and $pCO_2^{(oc)}$ are the partial presures in the atmosphere and the ocean, and V_p is a piston velocity. The product $V_p k_0$ is the gas transfer coefficient. In the experiments reported here the atmospheric pCO_2 is either held constant, or else the atmosphere is treated as a single well-mixed box. Spatial variations in atmospheric pCO_2 are thus neglected, which is a reasonable approximation for simulations which neglect seasonal variation since the lower atmosphere becomes well-mixed over a timescale of about a year (IPCC, 1990). The observed annual mean concentration difference between northern and southern hemispheres is 4 to 5 ppm. The southern hemisphere shows little annual variation in atmospheric CO_2 whilst the northern hemisphere shows variations of up to 10 ppm peak to peak amplitude towards the poles, which is thought to be due to seasonal changes in plant metabolism (Pearman *et al*, 1983). For seasonal simulations the neglect of atmospheric variations may therefore lead to errors in the calculated ΔpCO_2 of several ppm in some places but this is small when compared with the observed values of up to 100ppm. Seasonal changes in air-sea exchange are dominated by variations in the oceanic partial pressure. A more complete treatment of air-sea exchange would require the use of an atmospheric transport model and the inclusion of the terrestrial biosphere, which is beyond the scope of this paper.

The piston velocity, V_p, is computed from wind-speed according to the Liss and Merlivat (1986) formulation:

$$V_p = (S_c/600)^{-2/3}\, 0.17\, U \qquad U < 3.6\ ms^{-1}$$
$$V_p = (S_c/600)^{-1/2}\, (2.85\, U - 9.65) \qquad 3.6\ ms^{-1} \le U < 13.0\ ms^{-1} \qquad (13)$$
$$V_p = (S_c/600)^{-1/2}\, (5.9\, U - 49.3) \qquad 13.0\ ms^{-1} \le U$$

where S_c is the Schmidt number. The Schmidt number is a measure of the competing effects of gas diffusion and fluid viscosity on gas transfer and is calculated from the formula given by Wanninkhof (1992):

$$S_c = 2073.1 - 125.62\, T + 3.6276\, T^2 - 0.043219\, T^3 \qquad (14)$$

Apart from it's direct effects on pCO_2 (higher temperatures cause high values of pCO_2), temperature affects the flux across the air-sea interface. High temperatures result in low solubility and a lowering of the flux into the

ocean, which is partially offset by an increased flux due to a decreased Schmidt number. The piston velocity increases with increasing wind-speed - an abrupt increase in flux as wind speed exceeds 13 ms^{-1} represents the increase in turbulence brought about by breaking waves. Owing to the non-linearity of equation (13), for any given averaging period, a piston velocity calculated using an average wind speed will tend to be less than the average piston velocity for that period. Thus the use of monthly climatological winds to force the model will result in an underestimate of the gas transfer as compared with the case where the winds are variable. Wanninkhof (1992) has recently produced a new formulation of piston velocity which gives somewhat higher values than the ones used here. However, sensitivity studies by Sarmiento *et al* (1992) showed that, for annual mean forcing at least, global CO_2 uptake is relatively insensitive to the gas exchange formulation. We therefore retain the Liss and Merlivat (1986) formulation, which is commonly used. Over regions of the ocean covered by sea-ice, the atmosphere-ocean flux is drastically reduced since the flux at each grid box given by equation (12) is multiplied by the ice-free fractional area of that grid box. The only communication between ocean and atmosphere at ice points is through the small portion of a grid box representing leads and polynyas.

In addition to TCO2, ^{14}C is included as a passive tracer in a similar manner to that used by Toggweiler *et al* (1989), using a half-life of 5730 years and an arbitrary fixed atmospheric composition of 100 model units to represent the pre-industrial atmosphere. Results are reported in the conventional units as the per mil difference from the $^{14}C/C$ ratio of the pre-industrial atmosphere by the conversion

$$\Delta^{14}C = (\text{model units} - 100) / 10 \qquad (15)$$

The gas exchange rate is variable, according to the wind-speed dependent piston velocity computed in equation (13).

3 EXPERIMENTS

Initial fields of temperature and salinity were set from the Levitus (1982) climatology, TCO2 was initialised to a constant value of 2300 $\mu mol\ kg^{-1}$, $\Delta^{14}C$ was set to -150 ‰, and the model was spun up from a state of rest using the spin-up acceleration techniques described by Bryan (1984). In these, the model physics are distorted by taking a longer timestep for tracers than for the momentum equation and by taking longer timesteps at depth. This can be done because stability criteria are less severe for tracers and at depth within the ocean. The effect of the longer timestep at depth is to increase the effective integration time of the deep ocean relative to the surface. These techniques introduce scaling factors into the time-dependent terms of the equations of motion,

which tend towards zero as equilibrium is reached (d/dt = 0). Thus the equilibium state of a model integrated using spin-up acceleration will be the same as that of a model integrated with standard time-stepping, provided that the forcing used is steady. This results in a considerable saving in computer resources.

The model was spun up with accelerated time-stepping for 1200 surface years (equivalent to 9600 years in the deep ocean) using annual-mean forcing (spin-up stage I). Then synchronous timestepping was adopted with the same timestep being used at all depths and the spin-up was continued for a further 50 years (spin-up stage II). Atmospheric pCO_2 was held at a constant value of 348 ppm for the duration of the spin-up, corresponding to the value observed during the middle period of the 1980's. From year 1250 the model was integrated for a further 36 years with seasonal forcing imposed (spin-up stage III). By the end of the spin-up run the model property distributions had reached essentially steady state and the upper layers had come into equilibrium with the imposed seasonal forcing and atmospheric partial pressure (see discussion in section 4.1). By this time the net ocean-atmosphere carbon exchange was less than 0.05 GtC yr^{-1}.

Starting from the end of the seasonal spin-up (stage III) at model year 1286 an experiment was performed in which the atmospheric pCO_2 was no longer prescribed, but was allowed to vary as it exchanged CO_2 with the ocean. This will be referred to as experiment A. For the purposes of this run the atmosphere was treated as a single large well-mixed reservoir of such a size that the mid-1980's partial pressure of 348 ppm corresponded to an inventory of 750 GtC. At each timestep the atmospheric inventory was updated according to the fluxes to and from the ocean, and changes in atmospheric concentration were calculated as being proportional to the changes in inventory. In addition from model year 1286 onwards, CO_2 was continually added to the atmospheric reservoir at a constant rate of 5.4 GtC yr^{-1} to represent fossil fuel emissions. The rate at which CO_2 was added to the atmosphere is appropriate for the mid-1980's and the assumption of no increase in the rate corresponds to emission scenario D of the IPCC (1990) report. The purpose of this run was to look at the uptake of fossil fuel CO_2 by the ocean by comparing the results with those obtained at the end of the spin-up. The results, whilst not directly applicable to the present day uptake of CO_2, should give some idea of the proportion of anthropogenic CO_2 that the ocean can absorb and the time scale over which absorption occurs.

A further run was carried out, starting from the end of stage II of the spin-up at model year 1250, in which fossil fuel CO_2 was added to the atmospheric reservoir at the rate of 5.4 GtC yr^{-1} as before but this time annual mean forcing was used instead of seasonal forcing. This will be referred to as experiment B and was done in order to separate out the effects of seasonality. Note that experiments A and B start from different baseline carbon exchange figures, which needs to be taken account of in the comparison. Ideally, we would have liked to have

run the model with constant CO_2 until the net flux had settled down to a figure below 0.1 GtC yr^{-1} for both simulations. However this would have required an excessive amount of computer time as the net carbon flux in the annual-mean run was decreasing at a very slow rate of 0.004 GtC yr^{-1} by year 1250.

Another run was performed in which spin-up stages I and II and experiment B were repeated, but with a smaller value of the background vertical diffusion coefficient (0.1 $cm^2 s^{-1}$ instead of 0.5 $cm^2 s^{-1}$). This is known as experiment C and a comparison with experiment B (which is otherwise identical) will reveal the influence of changing the vertical diffusivity.

All of the experiments described here were run in ocean-only mode. That is, atmospheric forcing is prescribed from climatology and is not allowed to respond to changes in the ocean model. Although the ultimate aim of this work is to provide us with an ocean carbon cycle model that can interact with and provide feedback to the atmosphere, we have chosen in the first instance to omit these feedbacks in order to keep the model as simple as possible. The development of the model in a coupled ocean-atmosphere context will be explored in future studies.

4 RESULTS AND DISCUSSION

4.1 The Ocean Circulation Model

Before looking at the output from the carbon cycle model itself, it is instructive to examine some of the physical model output fields as these have a large effect on the CO_2 flux distributions to be seen later. Murphy (1994) provides additional discussion of the performance of an older, but essentially similar,version of the Hadley Centre model in the context of coupled modelling.

The total length of the spinup was 1250 years at the surface, and the equivalent of nearly 10,000 years in deep water, under annually-averaged forcing. A further 37 years was completed under seasonal forcing conditions. The portion of the run devoted to seasonal forcing was relatively short, the length of run being limited by

computational expense. Complete adjustment of the deep ocean to the imposition of seasonal forcing is not possible, owing to the long timescales (on the order of centuries to millenia) associated with the deep circulation. However the surface layers of the ocean, which are arguably the most important on the timescale of these experiments, come into equilibrium quite rapidly. This is illustrated by Figure 1 which shows the change in globally-averaged temperatures for selected layers over the entire period of seasonal forcing, normalised by the total change over the period. By the time the perturbation experiment commences, at model year 1287, the curves for the top 10 layers (300m and above) have levelled off. Lower down, the curves show no sign of levelling out over the course of the run, indicating that the deep water is still some way from achieving a new equilibrium state. The maximum change in temperature occurs at 666m, which cools at a rate of 0.24 ^{0}C per century. At 1500m the ocean warms by 0.074 ^{0}C per century. The trends in absolute terms are thus quite small, and have little effect on the model's thermohaline circulation. Figure 2 illustrates this point, by showing the zonally averaged annual-mean meridional streamfunction at the beginning and end of experiment A. Despite being 50 years apart, there is little difference between the two plots, other than a slight diminishing in strength of the cell that occurs in the northern hemisphere between 500m and 1000m depth.

The field which has the most obvious bearing on the carbon cycle is the sea surface temperature, shown in Figure 3 for four 3-monthly periods during year 1286, the final year of the spinup run. Because it determines the solubility of gaseous CO_2 in the sea water, it is important that the ocean model gives a good description of SST. The familiar pattern of warm water in the tropics with a relatively cold tongue in the east Pacific can be readily seen, and the SST pattern exhibits a marked latitudinal shift with the seasons, particularly in mid-latitudes. Also noticeable is the effect of season on the extent of ocean covered by sea-ice (ice-covered regions are shaded in Figure 3). Ocean-atmosphere gas flux is effectively cut off by the covering of sea-ice in the Arctic and Southern oceans and the extent of this is strongly dependent upon time of year. The simulation of SST is of course not a test of the model, since the restoring term in equation (6) prevents the model from doing anything other than predict the correct SST. Nevertheless, we show the plots because of the importance of SST in determining pCO_2.

Another field of direct interest to the carbon cycle is the meridional streamfunction (Figure 2a) which shows the zonally averaged movement of water in the meridional plane. Apart from the shallow wind-driven 'Ekman cells' in low latitudes the most striking features are the deep convective cells found at high latitudes in the North Atlantic and Southern Oceans. Deep water formation occurs adjacent to Antarctica in the Southern hemisphere and downwelling is also found to the north of the circumpolar westerlies at about 40° S. In the northern hemisphere deep convection takes place in the Labrador and Nordic seas, although Figure 2 tends to obscure the

North Atlantic deep circulation as it is zonally averaged. These features are illustrated further in Figure 4 which shows the depth of the mixed layer during March and September. Mixed layer depths in excess of 500m are picked out by light stippling, whilst areas covered by sea-ice are shown in cross-hatching. Surface water is mixed down to depths exceeding 500m in the Norwegian Sea and to the south of Greenland during March in close agreement with observations. In the southern hemisphere the model also has a large region to the south-west of Australia where the winter-time mixing extends down to more than 500 metres, which is absent from observations. Elsewhere, the model's mixed layer depths agree quite well with the maps published by Levitus (1982, Figs 95a and 96a). There is a tendency for the model to over-predict mixed layer depths in the tropics, and this may be related to the use of the Hellerman and Rosenstein wind stresses to force the model, since these are known to be too strong in this region. Generally, though, the model's seasonal mixing characteristics appear to be fairly representative of the real ocean.

It is particularly important that a model that aims to simulate the uptake of gas from the atmosphere should represent ocean ventilation processes realistically and give a reasonable description of the formation of deep water. Figures 5a and 5b show cross-sections of the annually-averaged zonal mean temperature for two runs of the model with different vertical diffusion coefficients, and Figure 5c shows the observed distribution, taken from Levitus (1982). In the standard run (Fig 5a) the model's thermocline is too deep and too diffuse. Also, the water just beneath the thermocline is too warm by as much as 3 °C, most obviously south of the equator and in northern mid-latitudes. This results in the subpolar fronts being much steeper than observed. The model does at least manage to capture some of the features of the observed distribution quite well, particularly the vertically well-mixed region around 60 °N and the north-south gradient in temperature in the southern hemisphere deep water. The low diffusivity run (Fig 5b) is discussed in section 4.3. Modelled and observed salinity sections for the Atlantic are shown in Figure 6. The model's source of Antarctic Bottom Water (AABW) close to the coast of Antarctica, which should have a salinity of 34.7 psu, is too fresh by about 0.5 psu and this allows Antarctic Intermediate Water (AAIW) of salinity around 34.5 psu to sink down to the bottom. The freshness of the model AABW is most likely due to the fact that the model's surface salinity is relaxed back towards the Levitus data, which is known to be too fresh close to Antarctica since the data is biased towards summertime values (England, 1992). Water of northern origin, such as North Atlantic Deep Water (NADW), which would normally occupy the bulk of the basin, has been restricted to depths shallower than 2500m owing to it's source water in the Norwegian Sea being too fresh and too warm during the long spin-up phase with annual-mean forcing. In the seasonally-forced part of the run the source water for NADW is produced only in the winter and it's TS characteristics are thus more like those found in reality. Unfortunately a long spin-up run involving seasonal forcing, which would be necessary to give the correct salinity structure in the Atlantic, would be

prohibitively expensive in computer time, since the techniques of split timestepping and deep-water acceleration may be inappropriate for non-steady forcing.

The model's simulation of the global water masses clearly leaves a lot to be desired. This appears to be a common feature among climate-resolution GCMs forced at the surface by annual mean climatology. The models of Toggweiler *et al* (1989) and Maier-Reimer and Hasselmann (1987) have similar difficulties in reproducing the observed salinity and tracer patterns. More encouraging is the presence in this model of a tongue of fresher water at 1000m in the southern hemisphere which extends as far north as the equator. This is intermediate water, and its appearance may be due to the fact that the bathymetry across Drake Passage is quite realistic, in contrast to models of coarser resolution. England (1992) found that the adjustment of the bathymetry of Drake Passage in a coarse resolution model, so that the tip of South America presented more of a barrier to circumpolar flow, resulted in a weakening of the wind-driven Deacon cell and an improvement in the northward penetration of AAIW.

As well as temperature and salinity sections, we also present the distributions of natural (ie. pre-bomb) radiocarbon computed by the model. Figure 7 shows a map of surface values. Highest $\Delta^{14}C$ values are found in the subtropics, reflecting the longer times for which water is at the surface. The lowest values are close to the coast of Antartica, where $\Delta^{14}C$ reaches -90 ‰, some 10‰ higher than estimates of the surface pre-industrial concentrations given by Broecker and Peng (1982). The average value over the region 30N to 30S is -40‰, in excellent agreement with estimates made by Toggweiler et al (1989) based on coral measurements. Figure 8 shows meridional sections through the Atlantic and Western Pacific oceans. The Pacific has the oldest waters with lowest ^{14}C concentrations of -240‰ on the bottom at 45 ^{0}N. The ^{14}C concentrations are comparable to those found in the Geosecs data (Broecker and Peng, 1982), but in the data the minimum occurs at about 2500m rather than on the bottom. The model captures the north-south slope of isolines in the deep water of the northern hemisphere which is seen in observations, but the deep water up against the coast of Antarctica has ^{14}C concentrations which are too high - 100‰, as compared with 160‰ seen in the observations - suggesting that the ventilation in this region may be too strong. Although the Pacific compares quite well with observations, the simulation in the Atlantic is less good. The ^{14}C concentration in the deepest part of the basin is too low by some 50‰ (cf. Broecker and Peng, 1982, fig. 5.5). The model produces North Atlantic Deep Water of the correct ^{14}C concentration (about -80‰), but it is unable to sink below 2500m, resulting in insufficient ventilation of the bottom water in the northern hemisphere. This same feature is seen in the salinity section shown in Figure 6a. In general, though, the model gives a reasonable simulation of the radiocarbon distribution. The model results resemble those obtained by Toggweiler *et al* (1989) in their experiment C, which were obtained using a rela-

tively high diffusivity of 1.0 cm^2s^{-1}.

The model predicts a Gulf stream transport of 38 Sv, similar to that observed (Knauss, 1969), and an Antarctic Circumpolar Current of strength 130 Sv, again close to observations (Nowlin and Klinck, 1986). Depth-mean flow through the Indonesian Passage is allowed in the model, and it's predicted strength is 24 Sv, which is somewhat larger than the estimate of 16 Sv given by the Sverdrup model of Godfrey (1989). One possible reason for this may be that the Indonesian sill, at 1200m, is too shallow, causing strong cross-sill pressure gradients to be set up (Hirst and Godfrey, 1993). The peak poleward heat transport is 0.99 Petawatts at 32.5 ^{0}N. This is lower than recent estimates of 3.75 and 1.5 Petawatts (Carrissimo *et al*, 1985; Hsuing, 1985), but is comparable to other models (eg Bryan and Lewis, 1979).

To summarise this section, whilst the modelled circulation characteristics appear reasonable, there are a number of areas where improvements are desirable. The deficiencies of the model highlighted in this section should be borne in mind when examining the uptake of gases.

4.2 The Carbon Cycle Model With Seasonal Forcing

We first of all look at the results from the steady state carbon cycle at the end of the seasonal spin-up run (stage III) before examining the model's uptake of anthropogenic CO_2.

4.2.1 The Steady-State Carbon Cycle

Figure 9 shows the surface TCO2 in µmol kg^{-1} at the end of the spinup (following the application of seasonal forcing). This plot is strongly related to the annual mean sea surface temperature pattern (not shown) with lowest carbon concentrations in the warm waters of the tropics and higher values in the cold waters of high latitudes. A tongue of higher TCO2 values is evident in the tropical east and central Pacific. There is very little variation in TCO2 in the model throughout the year, despite the strong seasonality of the SST field. The TCO2 pattern is essentially controlled by the long-term pattern of SST- at higher temperatures the partial pressure of CO_2 is higher, resulting in the loss of CO_2 to the atmosphere. Conversely, in cold water gas solubility is greater and the partial pressure is lower, encouraging the invasion of CO_2 from the atmosphere and thus higher concentrations. The air-sea gas exchange rate for CO_2 is slow (the equilibration time for CO_2 is ~ 1 year), and

thus seasonal changes in TCO2 caused by interaction with the atmosphere are slight. This absence of seasonality in TCO2 is in contrast to reality, where changes in TCO2 of order 100 μmol kg^{-1} can be observed, with lowest values in summer and highest values in winter caused by transport of deep water to the surface due to mixing (Takahashi *et al*, 1993). The model's seasonal variation does not exceed 5 μmol kg^{-1}. Figure 10 shows a zonally averaged vertical cross-section of the modelled TCO2 distribution. Whilst the surface values are well simulated, the deep ocean values are far too low. Deep water TCO2 as high as 2400 μmol kg^{-1} are observed in the oldest water of the Pacific. There is also no hint of the observed mid-depth maximum in equatorial waters at about 1000m. This deficiency is attributable to the neglect of ocean biology which tends to pass carbon rapidly from the surface in the form of sinking particles. Remineralisation of these particles increases the deep-water TCO2 and is responsible for the mid-depth maximum. The oldest waters have highest values of TCO2 since they have had more time to receive particles falling from the surface. Given the model's low deep water TCO2 concentration, we might expect our surface values of TCO2 to be too low in regions of strong upwelling and deep mixing. This results in the suppressed seasonal cycle in the model's surface TCO2. The other effect of biology is to cause a sharp decrease in TCO2 in the North Atlantic during spring and summer due to the spring bloom. This mechanism, absent from the model, also reduces the seasonal response.

The difference between the sea surface partial pressure of CO_2 and the atmospheric partial pressure of 348 ppm is plotted in Figure 11 for January-March and July-September. Regions where the oceanic partial pressure is lower than the atmospheric value, and CO_2 is liable to enter the ocean, are shaded. For comparison, Figure 12 shows a plot of ΔpCO_2 for observations made during the GEOSECS expedition. Summer conditions are shown for both hemispheres in this plot. Oceanic pCO_2 is greater than the atmospheric value in low latitudes, and lower in middle and high latitudes. The oceanic excess reaches values of between 60 and 80 ppm in the tropics and sub-tropics. Much of the middle latitudes show a deficit of 20 to 40 ppm whilst there are two regions of rather intense deficit as high as 80 ppm to be found in the north-west Atlantic and north-west Pacific, north of the Gulf Stream and Kuroshio currents during winter and spring. Lowest partial pressures are found around the coast of Antarctica and in the Arctic ocean, where deficits greater than 60 ppm are common, and values up up 120 ppm below the atmospheric value can be found during winter (not apparent from the plots). There is broad agreement between the modelled and observed pCO_2 differences, given the sparseness of the observations on which the data are based and taking into account the fact that the model values and observations represent slightly different times of year. However, a comparison of the model with more detailed seasonal data obtained over the past decade in the North and South Atlantic and North Pacific oceans (Takahashi *et al*, 1993) reveals a number of discrepancies which can be attributed to the lack of biology in this model. These data show high partial pressures in high latitudes during winter, with lower values in summer and a steep fall in partial pressure

in the North Atlantic at the time of the spring phytoplankton bloom. The higher winter values are associated with upwelling of deep waters rich in CO_2. In the model, on the other hand, the lowest partial pressures occur in winter at high latitudes, since variations in pCO_2 are dominated by sea surface temperature changes - winter upwelling of deep water has little effect on the model pCO_2 since the amount of CO_2 in deep water is too low. Owing to the neglect of biology, therefore, the seasonal cycle of model pCO_2 is of opposite phase to that seen in reality. Whether or not this failure of the model has a significant effect on uptake of excess anthropogenic CO_2 from the atmosphere remains to be seen. It may be that the seasonal variation of pCO_2 at a particular location is of little significance provided the annual average pCO_2 is correct. On the other hand, lower partial pressures during winter may favour a stronger flux of excess CO_2 into the ocean during that season due to stronger vertical mixing at that time of year. This is an issue that will be resolved once biology is introduced into the model.

Figure 13 shows the gas flux between atmosphere and ocean. The gas flux is governed mainly by the difference in partial pressures between atmosphere and ocean, but is also dependent on wind speed according to the Liss and Merlivat formula (equation (13)). Thus CO_2 leaves the ocean in the tropics and subtropics at a rate of up to 2 mol m^{-2} yr^{-1} and invades the ocean in the North Atlantic, the North Pacific and the Southern and Arctic oceans. Intense regions of strong invasion (up to 7 mol m^{-2} yr^{-1}) are found in winter in the North West Atlantic and Pacific where the strong winds in the path of the mid-latitude storm tracks amplify the effect of the peaks in air-sea pCO_2 difference found there. Although less intense, the Southern Ocean appears to be an important sink owing to the large area over which CO_2 is entering the ocean, particularly in the Indian Ocean sector where the wintertime mixing extends down to around 500m (Fig 4b). Notice also that although by far the lowest values of oceanic pCO_2 were found in the Arctic ocean and immediately adjacent to the coasts of Antarctica, very little exchange with the atmosphere occurs in those regions as the sea is covered in ice and the CO_2 can only invade the ocean through leads and polynyas in the ice. A very strong seasonal variation is evident, as can be seen from a time-latitude plot of the zonally averaged flux (Figure 14). The seasonality is much stronger in the northern hemisphere than in the south with the largest peak values occurring at 45° N. The intense atmosphere-to-ocean flux which occurs in late winter and early spring at 45° N is offset by a flux out of the sea in the same region during late summer and early autumn. The equatorial region remains a source to the atmosphere throughout the year, the southern-most part of the Southern Ocean and the extreme North Atlantic and Arctic ocean are sinks throughout the year, whilst much of the mid-latitudes can act as either a source or a sink for CO_2 depending on season. In particular, much of the North-West Pacific, which has the strongest uptake of any region during winter, acts as a weak source during the summer months. Outgassing from the ocean can occur as far north as 70° N, whilst the southern hemisphere acts as a sink throughout the year south

of 50° S. Over the whole globe the net air-sea flux is close to zero (less than 0.05 GtC yr^{-1}).

4.2.2 Uptake Of Anthropogenic CO_2

We turn now to experiment A and the uptake of anthropogenic CO_2 by the model ocean. Figure 15 shows the globally-averaged net flux of CO_2 from the atmosphere into the ocean during the seasonally forced part of the integration. The seasonal cycle has been removed from this figure by averaging over a period of a year. Until year 1286 the net flux is less than 0.05 GtC yr^{-1}, at which point CO2 is added to the well-mixed atmospheric box at a rate of 5.4 GtC each year. There is an initially rapid rise in the carbon flux into the ocean over the next 10 or so years, which begins to level out . By year 1336, after 50 years of CO_2 being added to the atmosphere, the net flux is 2.4 GtC yr^{-1}. At this point, the net flux is rising at a rate of just 0.007 GtC yr^{-1}. Over a 50 year period, then, the ocean has adjusted to the extra CO_2 emissions so that it is taking up 44% of the annual output - an airborne fraction of 0.56. Our results support the high uptake figures obtained with other ocean models - indeed this model predicts a slightly higher uptake than those reported previously (see, eg. Maier-Reimer and Hasselmann, 1987; Sarmiento et al, 1992). Our results suggest that, given enough time to adjust to the anthropogenic emission scenario, the ocean is capable of absorbing greater than 40 % of anthropogenic carbon if the influence of biological effects on the basic carbon cycle climatology is omitted.

There is, as one might expect, substantial temporal and spatial variation in the uptake of anthropogenic CO_2 simulated by the model. Figure 16 shows maps of the air-sea flux of excess CO_2 after 50 years of experiment A averaged over two three-month periods: January-March and July-September. The zonally averaged Hovmuller plot of the same quantity is plotted as Figure 17. Excess CO_2 flux is calculated as the difference between the fluxes obtained during experiment A and those obtained at the end of the spin-up, before extra CO_2 was added to the atmosphere. The maps are therefore a direct measure of where the atmospheric CO_2 is entering the ocean. The strongest uptake of "anthropogenic" CO_2 takes place at 45° N on the western sides of the North Atlantic and North Pacific, and immediately south of Greenland and Iceland as well as in the Nordic Seas. Fluxes as high as 4 mol m^{-2} yr^{-1} are attained. However, these fluxes are highly seasonal, and the northern hemisphere contributes very little in the absorption of excess atmospheric CO_2 between May and September (Figure 17). In the southern hemisphere, peak values are generally lower (except for some isolated areas of high flux adjacent to the ice edge during the austral winter which are an artifact caused by interannual variations in the exact location of the ice edge and the method used of obtaining the excess flux by differencing). However,

a significant flux in excess of 0.75 mol m^{-2} yr^{-1} occurs throughout the year at all latitudes between 50° S and the ice edge. Excess CO_2 uptake in GigaTonnes of carbon per year summed over various regions of the world ocean are given in Table 3 for northern hemisphere winter and summer, and for the annual mean. Averaged over the year, the three northern regions (N Pacific, Atlantic Gyre and Atlantic Subarctic) account for roughly equal amounts of carbon, totalling 0.69 GtC yr^{-1} between them. The equatorial region, extending from 15 ^{0}N to 15 ^{0}S, accounts for 0.5 GtC yr^{-1}. This is at first sight rather surprising as the tropics is often thought of as a source region for CO_2 (see Figs 13 and 14). However, it simply means that when the extra CO_2 is added to the atmosphere, the equatorial oceans are releasing less CO_2 back to the atmosphere than before due to the reduced partial pressure difference between atmosphere and ocean. The largest sink for anthropogenic CO_2 according to this model occurs in the southern hemisphere where the Southern Gyres and Antarctic regions take up 0.7 and 0.6 GtC yr^{-1} respectively. The area south of 15 degrees south thus accounts for 54% of the total uptake of excess CO_2, whilst the tropics contributes a further 21% of the total. These figures are in broad agreement with the perturbation uptake simulation of Sarmiento *et al* (1992) although in their model the equatorial region takes up slightly more CO_2 (28%).

A comparison of CO_2 uptake between the Tans *et al* (1990) analysis and the present model is presented in Table 4. It is difficult to compare our model with the Tans *et al* (1990) figures directly, since we are looking at the response of the ocean to CO_2 added at a constant rate, whereas the Tans *et al* (1990) model is attempting to simulate the flux at a particular time in history. However, since our model's annually-averaged global uptake varies from zero to 2.4 GtC yr^{-1} over the course of the experiment, by choosing the moment when our uptake matches the Tans *et al* (1990) figure of 1.6 GtC yr^{-1}, and comparing the two models at this stage when the global figures are equal, we can concentrate on looking at differences in location and timing of CO_2 uptake. Table 4 gives the gross fluxes of carbon, inclusive of the undisturbed, "pre - anthropogenic", fluxes before the addition of extra CO_2. There are considerable differences between our model and Tans *et al*'s (1990) estimates of the annual uptake. Tans *et al* (1990) estimate that the southern gyres take up a massive 2.39 GtC yr^{-1}, whilst the model gives just 0.79 GtC yr^{-1} with a further contribution of 0.96 GtC yr^{-1} from the region around Antarctica. In the model the northern hemisphere assumes more importance in relation to the southern hemisphere compared with Tans *et al*'s (1990) estimates, absorbing about 70% of the southern hemisphere total. The model's equatorial region emits about 30% less CO_2 than the Tans *et al* (1990) estimate. The model also exhibits greater seasonal variation than the estimates. We do not support the high uptake of the southern gyres given by the observationally-based estimate. This is in accordance with atmospheric transport modelling studies by Tans *et al* (1990) and Keeling *et al* (1989). However, we do predict a fairly large sink of order 1 GtC yr^{-1} south of 50° S. Close agreement with the estimates in the tables for the southern hemisphere is perhaps not to be

expected owing to the sparseness of data in the South Pacific, South Indian and Southern Oceans, particularly in the southern winter. The northern hemisphere is much better sampled and we would expect the data to be better constrained there. However, here there may be substantial time variations in partial pressure which may not be well captured by the data. In particular, phytoplankton blooms may lower partial pressures by as much as 100 ppm during spring and summer, resulting in enhanced uptake by the ocean (or reduced evasion to the atmosphere). This process is not yet included in the model. It would tend to increase the modelled uptake during July to October providing better agreement with observations for this period. From January to April the northern hemisphere sink is much stronger than is suggested by the observations, particularly for the North Pacific. Again, the inclusion of biological processes would tend to bring the modelled uptake closer to the data-based estimates, through the increase in partial pressure caused by bringing up high-TCO2 water from depth. Thus the inclusion of biology might be expected to bring seasonal variations in the modelled fluxes into closer alignment with observations without necessarily affecting the net uptake of anthropogenic CO_2. Over the year the model's combined northern hemisphere sink strength is 1.2 GtC yr^{-1}, which is of comparable magnitude to the southern hemisphere value of 1.75 GtC yr^{-1} and the equatorial source of -1.2 GtC yr^{-1}.

Figure 18 compares the response of the various regions identified in Table 3 to the increase in atmospheric pCO_2. In the period immediately prior to model year 1286, the point at which atmospheric CO_2 concentrations started to increase, the Atlantic Subarctic, North Pacific and Antarctic regions are still adjusting to the change from annual mean to seasonal forcing which occurred at year 1250. This may be related to a change in high latitude convection characteristics and a greater influence of NADW on the global scale water masses under seasonal forcing conditions. Prior to year 1286 the largest portion (just over 40%) of the CO_2 emitted from the tropics is absorbed by the Antarctic region. The Atlantic Subarctic takes up 23% and the North Pacific and Southern Gyres each contribute about 16%. After year 1286 the Southern Gyres region shows an initially rapid rise in air-to-sea flux, but the uptake curve saturates after about 25 years, by which time this region is absorbing 12% of the excess CO_2 added to the atmosphere each year. The three northern hemisphere regions show more modest rises with each region contributing approximately equally to the combined northern uptake. A slight trend is still evident in each northern region at the end of the run. The Antarctic, south of 50° S, initially takes up carbon at a slower rate than its neighbouring area to the north, but unlike the Southern Gyres does not reach a plateau. By the end of 50 years, this area accounts for 12% of the "anthropogenic emissions" and the curve is still rising at a rate of 0.005 GtC yr^{-1}. The equatorial region also absorbs a significant proportion of the emissions and shows a rising trend of 0.003 GtC yr^{-1}. The regions with the longest response time to an atmospheric CO_2 increase are, as one might expect, those regions where deep water is being brought up to the surface to replenish water saturated with excess CO_2.

The plots shown thus far depict the movement of carbon into the surface of the ocean, but what happens to that CO_2 once it is absorbed in the mixed layer? Figure 19 shows meridional sections through the Pacific and Atlantic oceans of the excess CO_2 from experiment A. After 50 years the anthropogenic CO_2 has not penetrated below 1000m in the tropical Atlantic ocean, but north of 35° N and south of 35° S the anthropogenic signal has reached the bottom of the ocean. The deep North Atlantic in particular shows a significant increase in TCO2 of 20 μmol kg^{-1} in water as deep as 2000m (at 50 ^{0}N - off the plot). The highest increase in TCO2 of up to 40 μmol kg^{-1} occurs in the subtropical gyres above the thermocline and the typical bowl-shape of the thermocline beneath the subtropical gyres can be clearly seen. In the Indian and Pacific oceans anthropogenic CO_2 again reaches the ocean bottom in the Southern hemisphere. Excess CO2 can be seen as deep as 1500m in the equatorial Pacific. Anthropogenic CO_2 is taken up into deep water in the North Atlantic (through the formation of NADW) and throughout the Southern Ocean (in AABW and AIW formation). The greater intensity of NADW formation results in fairly high deep water concentrations in the northern north Atlantic but the area over which this occurs is necessarily rather small. The southern hemisphere deep water formation simulated by the model occurs over a much wider area and there is a very large volume of water which is available to absorb the excess CO_2. The southern hemisphere thus acts as a larger sink for anthropogenic CO_2 than the northern hemisphere in this model. A rough check on the plausibility of the model can be made by comparing the results with observationally-based estimates of excess TCO2 provided by Chen (1982a,1982b). These estimates for a central Pacific section and the Atlantic Geosecs section are shown in Figure 20. The comparison with the model is not exact since the model shows the response to 50 years of emissions at a constant rate of 5.4 GtC yr^{-1}, whilst the data reflects emissions rising over a period of almost 200 years from zero to 5.4 GtC yr^{-1}. The cumulative release of CO_2 from fossil fuel use from 1850 to 1987 is estimated at 200 GtC (Marland,1989), as compared with a total output of 270 GtC in the model. We can however compare the general shape of the sections. Figures 19 and 20 show reasonably good agreement. Comparison of Figure 19(b) with Figure 20(b) shows that the model's TCO2 penetration is slightly overstrong in the Southern Ocean and that the TCO2 originating in the North Atlantic does not extend as far south along the bottom as is observed. The reasons for this were discussed in section 4.1. Maier-Reimer and Hasselmann (1987) have greater penetration of excess TCO2 in the South Atlantic in their model, whilst the Sarmiento *et al* (1992) model shows very little. The behaviour of this model appears to lie somewhere between the two. In the North Pacific both the penetration and structure of the model results agree fairly well with the observations, indicating that the thermocline ventilation characteristics of the model are approximately correct.

4.3 Annual-mean Forcing - Comparison with Seasonal Forcing

The carbon cycle simulations reported thus far in the literature describe results obtained using annual-mean forcing. One of the purposes of this work was to examine the effects on CO_2 uptake of including seasonal variations. The previous sections showed the large variations throughout the year of pCO_2, ice cover and mixed layer depth. Gas exchange coefficient also undergoes marked seasonal variation through its dependence on the wind speed via the Liss and Merlivat formula (equation (13)). In mid-latitudes the winds are much stronger in winter than in summer which results in a larger gas exchange coefficient and a deeper mixed layer, resulting in a larger reservoir available for absorbing CO_2. pCO_2 is also lower in winter because of lower SSTs. Thus the flux into the ocean in winter when ΔpCO_2 is positive should be stronger than the summertime flux out of the ocean when ΔpCO_2 is negative. One might expect, therefore, the results from simulations that include the seasonal cycle to be somewhat different from those from a model forced with annually-averaged fields. To test this out, we performed a simulation, parallel to experiment A, in which atmospheric CO_2 is increased at the same rate as before, but the model is forced with an annually-averaged version of the climatology used to force experiment A. This annual-mean simulation is referred to as experiment B. Apart from their forcing, experiments A and B are otherwise identical. It is not quite as straightforward as one might wish to compare experiments A and B because they were started from different baselines. Experiment A was started from the seasonal stage of the spin-up at which time the global net CO_2 flux between atmosphere and ocean was 0.04 GtC yr^{-1} out of the ocean. Experiment B started from the annually-forced stage of the spin-up at which time there was a flux out of the ocean of 0.35 GtC yr^{-1}. Allowance has been made for the different starting points of the two experiments.

Figure 21 shows the atmosphere-ocean flux for the 50 years during which the seasonally- and annual-mean-forced experiments were run. The curves have been offset so that they both start from an initial flux of zero GtC yr^{-1}. After 5 years the curves start to diverge, but after 50 years the model takes up excess atmospheric carbon at a rate of 2.42 GtC yr^{-1} in the seasonally forced case compared with 2.53 GtC yr^{-1} in the annual-mean run - a difference of only 0.1 GtC yr^{-1}. One could, however, object to this interpretation on the grounds that the two stages of the spin-up immediately prior to the start of experiments A and B exhibit quite different trends, as can be seen from Figure 21. For the seasonal spin-up the atmosphere-ocean flux is decreasing at a rate of 0.001 GtC yr^{-1} whilst in the annual-mean spin-up the flux is increasing at 0.004 GtC yr^{-1} If these trends are removed from the curves of Figure 21 then the seasonally-forced model appears to be taking up carbon at a rate of 0.1 GtC yr^{-1} greater than in the annual-mean case. Whichever way we look at it, the use of annual mean as opposed to seasonal forcing has remarkably little effect on the global uptake of carbon by the ocean. By the end of 50 years

of emissions, the difference between the two runs is 0.1 GtC yr^{-1} - just 4% difference. We therefore conclude that, contrary to expectations, the inclusion of a seasonal cycle has little effect on the annual-mean, global uptake of CO_2. This seems somewhat surprising in view of the discussion above and the effect of seasonally varying ice cover and SSTs on North Atlantic Deep Water formation. The small influence of seasonality can perhaps be explained by the predominance of the southern hemisphere and the tropics in the absorption of excess CO_2 (Figure 18) combined with the effects of seasonality being confined more to the northern hemisphere as can be seen from Figure 17. The fluxes south of 30° N show relatively minor variations through the seasons.

4.4 The Effect Of Changing The Diffusivity

Bryan (1987) showed, in a series of experiments using simplified GCMs, that the thermohaline circulation of such models is very sensitive to the value used for the coefficient of vertical diffusivity. Higher diffusivity results in a thicker thermocline which causes stronger north-south pressure gradients to be set up at the depth of the thermocline, and this drives a stronger meridional circulation. The values of diffusivity typically used range from 0.1 $cm^2 s^{-1}$ to 1.3 $cm^2 s^{-1}$. The lower value tends to keep the thermocline thickness close to observations but results in a meridional circulation that is too sluggish. The higher value has a more realistic overturning but too diffuse a thermocline. In practice the value actually used tends to be based on a compromise between these two effects. What is represented as diffusion corresponds in the real ocean to a variety of processes, such as mixing by breaking internal waves, double diffusion, thermohaline staircases and so on. The dominant process varies from region to region as well as in time and so the use of a constant diffusion coefficient is a very crude parametrization. The same coefficient tends to be used for heat and salt, with little justification. Gargett and Holloway (1992) showed that models such as these are also sensitive to the relative magnitudes of heat and salt diffusivities if separate coefficients are used. Unfortunately it seems that some parts of the ocean will have stronger heat diffusion, whilst others will have stronger diffusion of salt depending on whichever physical process is dominant at any particular time. This makes the problem of parametrization even more acute.

In order to assess the impact on CO_2 uptake of poor knowledge of the vertical diffusion coefficient we performed another experiment, parallel to experiment B, in which the background vertical diffusivity of heat, salt and TCO2 was reduced from 0.5 $cm^2 s^{-1}$ to 0.1 $cm^2 s^{-1}$. All other aspects of the two experiments were identical. The run with the lower diffusion coefficient is referred to as experiment C. Both diffusivities are plausible values, lying at the mid- and low-ends of the commonly-used range of values. The meridional volume transport

for the global ocean for each experiment is shown in Figure 22. The wind-driven surface cells in the tropics and the two sub-surface cells have declined in strength by between 20 and 30% as the diffusivity has been decreased. The southerly Ekman cell is 500m shallower than before and the convective cell close to the coast of Antarctica has been lost. The Deacon cell centred at 45° S has changed little in maximum strength, and the deep cell centred at 15 ^{0}S is much less vigorous than before. Meridional sections of the zonally averaged excess TCO2 after 50 years of emissions are shown for the two experiments in Figure 23. For the higher diffusivity case, the thermocline is thicker and the 10 μmol kg^{-1} isoline is some 100m deeper in the tropics. The thermocline is less "bowl-shaped" in the northern hemisphere where the 10 μmol kg^{-1} isoline has deepened by 300m at 50° N, and the deeper penetration is particularly noticeable in the Southern Ocean. This rather simple change to the diffusivity coefficient has a dramatic effect on the global uptake of CO_2 by the ocean (Figure 24). For the first 5 years of emissions the two models take up CO_2 at roughly similar rates. Thereafter, the uptake rates diverge rapidly until by the end of 50 years, the low-diffusivity model is absorbing CO_2 at a rate of 0.4 GtC yr^{-1} less than in the high diffusivity case. A fairly minor reduction in a poorly-known parameter has resulted in a 20% reduction in CO_2 absorption. The stronger flux in experiment B is due partly to enhanced diffusion of CO2 away from the surface through the thermocline, and partly to the stronger overturning circulation. Figure 25 shows the difference between the fluxes in experiments B and C for each region. At the time when the emissions into the atmosphere started, enhanced evasion of CO_2 from the tropics into the atmosphere in experiment B was balanced by stronger invasion south of 15° S. As the runs proceeded, the equatorial and the southern hemisphere regions took up more carbon in experiment B than experiment C, whilst the northern regions showed relatively minor differences. By the end of 50 years the equatorial region accounted for 0.125 GtC yr^{-1}, the Southern Gyres 0.14 and the Antarctic 0.08 GtC yr^{-1} of the total difference between the runs of 0.4 GtC yr^{--1}. This suggests that the major cause of the enhanced uptake is the stronger southern hemisphere meridional circulation induced by higher diffusion.

Which of the two uptake rates is closest to reality? Both runs use diffusivities which are well within the range of those usually employed in models, but radiocarbon simulations may enable us to place constraints on the estimates. Figure 26 shows the natural radiocarbon distribution at the surface for the low diffusion experiment, C. Meridional sections from the same run are shown in Figure 27. These should be compared with the corresponding plots for experiment B, given in Figures 7 and 8. Surface ^{14}C concentrations are 10-20 ‰ lower in experiment C than experiment B, and the average value for the latitude range 30 ^{0}S-30 ^{0}N is -24 ‰, compared with observations of -40 ‰. For the low diffusion case, the deep water concentrations are far too low and the observed north-south gradient in the deep Pacific is conspicuously lacking. This is also apparent from a section of zonally-averaged temperature (Fig 5b). Thus it would appear that experiment C could be discounted on the

basis that it is unable to provide a satisfactorily simulation of deep water $\Delta^{14}C$, and that it's deep water ventilation characteristics are too sluggish. However, in some ways the low diffusivity simulation is preferable to the high one. The thermocline is shallower and less diffuse, and the radiocarbon distributions above about 2000m would appear to be more realistic. If it is believed that the region above the thermocline is more important for CO_2 uptake on the timescale of decades, then it could perhaps be argued that the low diffusivity run should provide the better estimate. The use of radiocarbon data to constrain the model is not without ambiguities.

5 SUMMARY AND CONCLUSIONS

In this paper we have described the development of a three-dimensional model of the ocean's inorganic carbon cycle within the context of an ocean general circulation model. The model is suitable for coupling to an atmospheric general circulation model for studies of climate change and has been designed with this pupose in mind. We presented results from a seasonal simulation of the present-day ocean carbon cycle. The circulation characteristics of the model appear reasonable, but a number of deficiencies in the model have been identified. In common with other GCMs, under conditions of annual mean forcing the model gives North Atlantic Deep Water formation rates that are too low in comparison with deep water of southern origin. It is likely that the use of a more realistic fresh water forcing over the Southern Ocean will improve matters since the forcing dataset employed for these integrations is known to be biased towards summertime values when surface salinities are fresher. The bias towards deep water formation in the southern hemisphere may result in an overestimate of the uptake of CO_2 by the southern oceans. A particular restriction of the model is the neglect of the role of ocean biology in the carbon cycle. Biological processes transfer carbon quite rapidly from surface waters into the deep ocean and are responsible for maintaining much higher concentrations of CO_2 in the deep ocean than is found at the sea surface. The omission of biology has two effects in the model. Firstly, the sharp fall in pCO_2 associated with the spring phytoplankton bloom that is observed in late spring/early summer in the North Atlantic and adjacent seas is not simulated, and summertime partial pressures are consequently too high. Secondly, the model gives deep TCO2 values that are far too low and this means that the high concentrations of CO_2 that are seen at the surface during winter under conditions of deep mixing are similarly not captured by the model. A detailed comparison between the model's simulated surface partial pressures and seasonal observations in high latitudes published by Takahashi *et al* (1993) is in consequence rather poor. The model gives lowest partial pressures during winter and highest in summer, since the partial pressure in the model is dominated by the seasonal cycle of sea surface temperature. Meanwhile, observations in high latitude oceans show the opposite - highest values in winter and lowest during summer. Work is in hand to include biology in

the next version of the carbon cycle model, and it is anticipated that this will markedly improve the simulation of the present-day carbon cycle.

We investigated the response of the model to a steady increase in anthropogenic CO_2 emissions into the atmosphere over a timescale of 50 years, under conditions of both seasonal and annual-mean forcing. Under seasonal forcing, after 50 years of the perturbation experiment, the ocean is absorbing 2.4 GtC yr^{-1} of the atmospheric emissions of 5.4 Gtc yr^{-1}, giving an airborne fraction of 0.56. These figures are similar to those obtained with other ocean models. The comparison of a control and a perturbation experiment allows us to see directly where the excess CO_2 has gone in the ocean. The southern hemisphere is the dominant region for uptake of excess CO_2 - the area south of 15°S accounts for 54% of the total uptake, whilst the northern oceans account for just 25%. This is partly because of the larger area of ocean south of the equator, and partly due to the stronger seasonality of air-sea fluxes in the northern hemisphere compared with the southern hemisphere - the northern oceans absorb very little anthropogenic CO_2 during late summer. It remains to be seen how these estimates will be changed when biology is included in the model. The Antarctic ocean, south of 50° S, and the equatorial region, between 15° N and 15° S, show the longest response times to the perturbation. Penetration of excess CO_2 below the surface shows quite reasonable agreement with observationally-based estimates. An attempt was also made to compare the model's predicted CO_2 uptake with the estimates of Tans *et al* (1990). The agreement was not good, but the comparison was hampered by the non-standard emissions scenario. The method used assumed that the relationship between the CO_2 uptake of different regions is fixed in time, and this assumption is clearly violated (see Figure 18). Also, inclusion of biology would tend to bring the seasonal variation in fluxes in high latitude regions closer to observations. We intend to carry out further experiments using the time-history of atmospheric pCO_2 to force the uptake, both with and without biology. This will enable a more meaningful comparison to be made.

The use of annual mean as opposed to seasonal forcing has surprisingly little effect on global uptake of CO_2. After 50 years of emissions the two experiments differed by less than 0.1 GtC yr^{-1} in their CO_2 uptake rates. This low sensitivity to the seasonal cycle may be due to the fact that 75% of the excess CO_2 uptake occurs south of 15° N, where the fluxes exhibit little seasonal variation. Again, the inclusion of biology may change this conclusion.

We have also looked at the sensitivity of the model results to variations in the vertical diffusion coefficient, although the high cost of performing lengthy integrations with a GCM has restricted the number of runs that could be done. Lowering the background vertical diffusion coefficient was found to have a much greater effect

on the estimated CO_2 uptake. Changing the diffusion coefficient for tracers, within a physically reasonable range, from 0.5 $cm^2\ s^{-1}$ to 0.1 $cm^2\ s^{-1}$ resulted in a 20% reduction in CO_2 uptake, which was associated with a weaker meridional circulation in the southern hemisphere. The simulation of deep water $\Delta^{14}C$ was very poor in the experiment which used the lowest diffusivity, which suggests that CO_2 uptake estimates based on this run would be too low. However, the simulation above 1000m was actually improved by reducing the diffusivity. In future, we may be able to improve the model by employing a diffusivity which varies from low values at the surface to higher values in deep water, as in Bryan and Lewis (1979). Simulation of bomb, as opposed to natural, radiocarbon would have been useful in deciding which diffusivity formulation to use, but this was not possible because of the way in which the carbon cyle model was forced. This sensitivity of CO_2 uptake to the choice of a poorly constrained parameter highlights the need for better parametrizations for sub-grid-scale phenomena.

The use of fully three-dimensional models for studies of the carbon cycle is still in it's infancy and many improvements and refinements to the models, in terms of both ocean physics and dynamics as well as the carbon cycle models themselves, can be expected in the future. This will eventually lead to improved understanding of the role of the carbon cycle in climate change.

ACKNOWLEDGEMENTS

The author would like to thank three reviewers whose suggestions helped improve the paper significantly.

The work described in this article was carried out at the Hadley Centre for Climate Prediction and Research under the UK Department of the Environment Climate Prediction Programme (contract PECD 7/12/37).

REFERENCES

Bacastow, R.B. (1981). Numerical evaluation of the evasion factor. In Carbon Cycle Modelling, edited by B. Bolin, pp 95-101, John Wiley, New York.

Bacastow, R.B., and Maier-Reimer, E. (1990). Ocean-circulation model of the carbon cycle. Clim. Dyn., 4, 95-125.

Bottomley, M., Folland, C.K., Hsiung, J., Newell, R.E., and Parker, D.E. (1990). Global ocean surface temperature atlas (GOSTA). A joint project of the Meteorological Office and Dept. of Earth, Atmospheric and Planetary Sciences, Massachusetts Institute of Technology. HMSO, London, 333pp.

Broecker, W.S., and Peng, T.H. (1982). Tracers in the sea. Lamont-Doherty Geological Observatory, Palisades, N.Y. 690pp.

Broecker, W.S., and Peng, T.H. (1992). Interhemispheric transport of carbon dioxide by ocean circulation. Nature, 356, 587-589.

Bryan, F. (1987). Parameter sensitivity of primitive equation ocean general circulation models. J. Phys. Oceanogr., 17, 970-985.

Bryan, K. (1969). A numerical method for the study of the circulation of the world ocean. J. Comput. Phys., 4, 347-379.

Bryan, K. (1984). Accelerating the convergence to equilibrium of ocean climate models. J. Phys. Oceanogr., 14, 666-673.

Bryan, K., and Cox, M.D. (1972). An approximate equation of state for numerical models of ocean circulation. J. Phys. Oceanogr., 2, 510-514.

Bryan, K., and Lewis, L.J. (1979). A water mass model of the world ocean. J. Geophys. Res., 84, 2503-2517.

Carrissimo, B.C., Oort, A.H., and Vonder Haar, T.H. (1985). Estimates of the meridional energy transports in the atmosphere and ocean. J. Phys. Oceanogr., 15, 82-91.

Chen, C-T. A. (1982a). On the distribution of anthropogenic CO_2 in the Atlantic and Southern oceans. Deep-Sea Res., 5, 563-580.

Chen, C-T. A. (1982b). Oceanic penetration of excess CO_2 in a cross section between Alaska and Hawaii. Geophys. Res. Lett., 9, 117-119.

Cox, M.D. (1984). A primitive equation, 3-dimensional model of the ocean. GFDL Ocean Group Tech. Rep. No. 1, 143pp.

Cox, M.D. (1987). Isopycnal Diffusion in a z-coordinate ocean model. Ocean Modelling, 74, 1-5. Unpublished Manuscript.

England, M.H. (1992). On the formation of Antarctic Intermediate and Bottom Water in ocean general circulation models. J. Phys. Oceanogr., 22, 918-926.

England, M.H. (1993). Representing the global-scale water masses in ocean general circulation models. J. Phys. Oceanogr., 23, 1523-1552.

Esbensen, S.K., and Kushnir, Y. (1981). The heat budget of the global ocean: An atlas based on estimates from surface marine observations. Climate Research Institute, Rep. No. 29, Oregon State University, Corvallis, USA.

Etcheto, J., and Merlivat, L. (1988). Satellite determination of the carbon dioxide exchange coefficient at the ocean-atmosphere interface: A first step. J. Geophys. Res., 93, 15669-15678.

Fieux, M., Andre, C., Delecluse, P., Ilahude, A.G., Kartavseff, A., Mantisi, F., Molcard, R., and Swallow, J.C. (1994). Measurements within the Pacific- Indian oceans throughflow region: preliminary results of the

JADE cruise. Deep-Sea Res., in press

Gargett, A.E., and Holloway, G. (1992). Sensitivity of the GFDL ocean model to different diffusivities for heat and salt. J. Phys. Oceanogr., 22, 1158-1177.

Godfrey, J.S. (1989). A Sverdrup model of the depth-integrated flow for the world ocean allowing for island circulations. Geophys. Astrophys. Fluid Dyn., 45, 89-112.

Goyet, C., and Poisson, A. (1989). New determination of carbonic acid dissociation constants in seawater as a function of temperature and salinity. Deep Sea Res., 36, 1635-1654.

Haney, R.L. (1971). Surface thermal boundary condition for ocean circulation models. J. Phys. Oceanogr., 1, 241-248.

Hellerman, S., and Rosenstein, M. (1983). Normal monthly wind stress over the world ocean with error estimates. J. Phys. Oceanogr., 13, 1093-1104.

Hibler, W.D. (1979). A dynamic-thermodynamic sea-ice model. J. Phys. Oceanogr., 9, 815-846.

Hirst, A.C., and Godfrey, J.S. (1993). The role of Indonesian throughflow in a global ocean GCM. J. Phys. Oceanogr., 23, 1057-1086.

Hsuing, J. (1985). Estimates of global oceanic meridional heat transport. J. Phys. Oceanogr., 15, 1405-1413.

IPCC (1990). Climate Change: the IPCC Scientific Assessment. J.T. Houghton, G.J. Jenkins, and J.J. Ephraums (Eds.), Cambridge University Press, Cambridge, UK, 365pp.

Jaeger, L. (1976). Monatskarten des Niederschlags fur die Ganze Erde. Ber Deutsch Wetterdienstes, 18, no. 139.

Kraus, E.B., and Turner, J.S. (1967). A one-dimensional model of the seasonal thermocline. II. The general

theory and its consequences. Tellus, 19, 98-105.

Keeling, C.D., Piper, S.C., and Heimann, M. (1989). A three dimensional model of atmospheric CO_2 transport based on observed winds, 4, Mean annual gradients and interannual variations. In Aspects of Climate Variability in the Pacific and the Western Americas, edited by D.H. Peterson, pp305-363, AGU, Washington, D.C.

Keeling, R.F., and Shertz, S.R. (1992). Seasonal and atmospheric variations in atmospheric oxygen and implications for the global carbon cycle. Nature, 358, 723-727.

Knaus, J. (1969). A note on the transport of the Gulf Stream. Deep Sea Res., 16, suppl., 117-124.

Levitus, S. (1982). Climatological Atlas of the World Ocean, NOAA Professional Paper 13, U.S. Dept. of Commerce, 173pp.

Liss, P., and Merlivat, L. (1986). Air-sea gas exchange rates, introduction and synthesis. In The Role of Air-Sea Exchange in Geochemical Cycling, edited by P. Buat-Menard, pp 113-128, D.Reidel, Dordrecht .

Maier-Reimer, E., and Hasselmann, K. (1987). Transport and storage of CO_2 in the ocean - An inorganic ocean-circulation carbon cycle model. Clim. Dyn., 2, 63-90.

Manabe, S., and Stouffer, R. (1988). Two stable equilibria of a coupled ocean-atmosphere model. J. Climate, 1, 841-866

Marland, G. (1989). Fossil fuels CO_2 emissions. CDIAC Communications, Winter 1989,pp1-3, Carbon Dioxide Information Analysis Center, Oak Ridge National Laboratory, Oak Ridge, Tenn.

Mehrbach, C., Culberson, C.H., Hawley, J.E., and Pytkowicz, R.M. (1973). Measurement of apparent dissociation constants of carbonic acid in seawater at atmospheric pressure. Limnol. Oceanogr., 18, 897-907.

Murphy, J. (1994). Transient response of the Hadley Centre coupled ocean-atmosphere model to increasing carbon dioxide. Part I. Control climate and flux correction. Journal of Climate. In Press

Nowlin, W.D. Jr., and Klinck, J.M. (1986). The physics of the Antarctic Circumpolar Current. Reviews of Geophysics, 24, 469-491.

Pacanowski, R.C., and Philander, S.G.H. (1981). Parametrization of vertical mixing in numerical models of tropical oceans. J. Phys. Oceanogr., 11, 1443-1451.

Paulson, C.A., and Simpson, J.J. (1977). Irradiance measurements in the upper ocean. J. Phys. Oceanogr., 7, 952-956.

Pearman G.I., Hyson, P., and Fraser, P.J. (1983). The global distribution of atmospheric carbon dioxide. J. Geophys. Res., 88, 3581-3590.

Peng, T-H., Takahashi, T., and Broecker, W. (1987). Seasonal variability of carbon dioxide, nutrients and oxygen in the northern North Atlantic surface water: observations and a model. Tellus, 39B, 439-458.

Redi, M.H. (1982). Oceanic isopycnal mixing by coordinate rotation. J. Phys. Oceanogr., 12, 1154-1158.

Roberts, D.L., and Cattle, H. (1989). Simulation of sea-ice in a coupled ocean-atmosphere model. Met O 20 Dynamical Climatology Technical Note No. 85. Meteorological Office, Bracknell, U.K.

Robertson, J.E., and Watson, A.J. (1992). Thermal skin effect of the surface ocean and its implications for CO_2 uptake. Nature, 358, 738-740

Sarmiento, J.L., and Sundquist, E.T. (1992). Revised budget for the oceanic uptake of anthropogenic carbon dioxide. Nature, 356, 589-593.

Sarmiento, J.L., Orr, J.C. and Siegenthaler, U. (1992). A perturbation simulation of CO_2 uptake in an ocean general circulation model. J. Geophys. Res., 97, 3621-3645.

Semtner, A.J. (1976). A model for the thermodynamic growth of sea ice in numerical investigations of climate. J. Phys. Oceanogr., 6, 379-389.

Takahashi, T., and Azevado, A.E.G. (1982). The oceans as a CO_2 reservoir. In: Interpretation of climate and photochemical models, ozone and temperature measurements. American Institute of Physics. New York.

Takahashi, T., Olafsson, J., Goddard, J.G., Chipman, D.W., and Sutherland, S.C. (1993). Seasonal variation of CO_2 and nutrients in the high latitude oceans: a comparative study. Global Biogeochemical Cycles, 7, 843-878.

Tans, P.P., Fung, I.Y. and Takahashi, T. (1990). Observational constraints on the global atmospheric CO_2 budget. Science, 247, 1431-1438.

Taylor, N.K. (1992). The role of the ocean in the global carbon cycle. Part 2: Climate feedbacks. Weather, 47, 237-241.

Thomas, F., Perigaud, C., Merlivat, L. and Minster, J.F. (1988). World scale monthly mapping of the CO_2 ocean-atmosphere gas transfer coefficient. Philos. Trans. R. Soc. London Ser. A, 325, 71-83.

Toggweiler, J.R., Dixon, K., and Bryan, K. (1989). Simulations of radiocarbon in a coarse-resolution, world ocean model. I.Steady state, pre-bomb dostributions. J. Geophys. Res., 94, 8217-8242

Wanninkhof, R. (1992). Relationship between wind speed and gas exchange over the ocean. J. Geophys. Res., 97, 7373-7382.

Watson, A.J., Robinson, C., Robertson, J.E., Williams, P.J.le B. and Fasham, M.J.R. (1991). Spatial variabiity in the sink for atmospheric carbon dioxide in the North Atlantic. Nature, 350, 50-53.

Yin, F.L., and Fung, I.Y. (1991). Net diffusivity in ocean general circulation models with nonuniform grids. J. Geophys. Res., 96, 10773-10776.

TABLES

TABLE 1 : MODEL LEVELS

Level	Thickness (m)	Depth of level bottom (m)	Depth of mid-point (m)
1	10.0	10.0	5.0
2	10.0	20.0	15.0
3	10.0	30.0	25.0
4	10.2	40.2	35.1
5	15.3	55.5	47.8
6	23.0	78.5	67.0
7	34.5	113.0	95.7
8	51.8	164.8	138.9
9	77.8	242.6	203.7
10	116.8	359.4	301.0
11	175.3	534.7	447.0
12	263.2	797.9	666.3
13	395.3	1193.2	995.5
14	615.3	1808.5	1500.8
15	615.3	2423.8	2116.1
16	615.3	3039.1	2731.3
17	615.3	3654.4	3346.6
18	615.3	4269.7	3961.9
19	615.3	4885.0	4577.1
20	615.3	5500.3	5192.4

TABLE 2 : OCEAN MODEL PARAMETER SETTINGS

Background vertical eddy viscosity	υ_b	cm^2s^{-1}	0.1
Background vertical eddy diffusivity	χ_b	cm^2s^{-1}	0.1 , 0.5
Vertical eddy viscosity under conditions of neutral stability	υ_0	cm^2s^{-1}	55.0
Maximum vertical eddy viscosity under unstable conditions		cm^2s^{-1}	100.0
Adjustable parameters in the K-theory mixing scheme	α		5
	n		2
Minimum horizontal viscosity	A_{m1}	cm^2s^{-1}	1.5×10^9
Additional horizontal viscosity at equator	A_{m2}	cm^2s^{-1}	1.5×10^9
Surface isopycnal diffusivity	A_s	cm^2s^{-1}	2.0×10^7
Background isopycnal diffusivity	A_b	cm^2s^{-1}	0.4×10^7
Depth-scale for decay of isopycnal diffusivity to background level		m	500.0
Maximum slope of isopycnal surfaces			1.0×10^{-2}
Background horizontal diffusivity		cm^2s^{-1}	8.0×10^5
Relaxation coefficient for surface temperature and salinity	λ	$Wm^{-2}K^{-1}$	40.9
Attenuation coefficient for long-wave component of penetrative solar radiation	η_1	m^{-1}	1.0
Attenuation coefficient for short-wave component of penetrative solar radiation	η_2	m^{-1}	0.059
Proportion of penetrative solar radiation in long-wave band			0.67

TABLE 3 : OCEANIC UPTAKE OF EXCESS CO2 AFTER 50 YEARS OF EMISSIONS

REGION	January to April	July to October	Annual Mean
Atlantic Subarctic	0.3	0.1	0.2
Atlantic Gyre	0.4	0.1	0.2
North Pacific	0.4	0.0	0.2
Equatorial	0.5	0.6	0.5
Southern Gyres	0.3	1.0	0.7
Antarctic	0.5	0.7	0.6
Global	2.4	2.5	2.4

TABLE 4 : ATMOSPHERE-OCEAN CO2 FLUX : COMPARISON OF MODEL WITH OBSERVATIONALLY-BASED ESTIMATES OF TANS *et al* (1990)

REGION	January to April		July to October		Annual Mean	
	Model	Tans	Model	Tans	Model	Tans
Atlantic Subarctic	0.89	0.15	0.07	0.31	0.51	0.23
Atlantic Gyre	0.80	0.58	-0.23	0.02	0.23	0.30
North Pacific	1.28	0.44	-0.43	-0.33	0.46	0.06
Equatorial	-1.15	-1.56	-1.10	-1.69	-1.17	-1.62
Southern Gyres	-0.47	1.46	1.99	3.31	0.79	2.39
Antarctic	0.64	0.38	1.26	0.03	0.96	0.20
Global	1.56	1.5	1.55	1.7	1.59	1.6

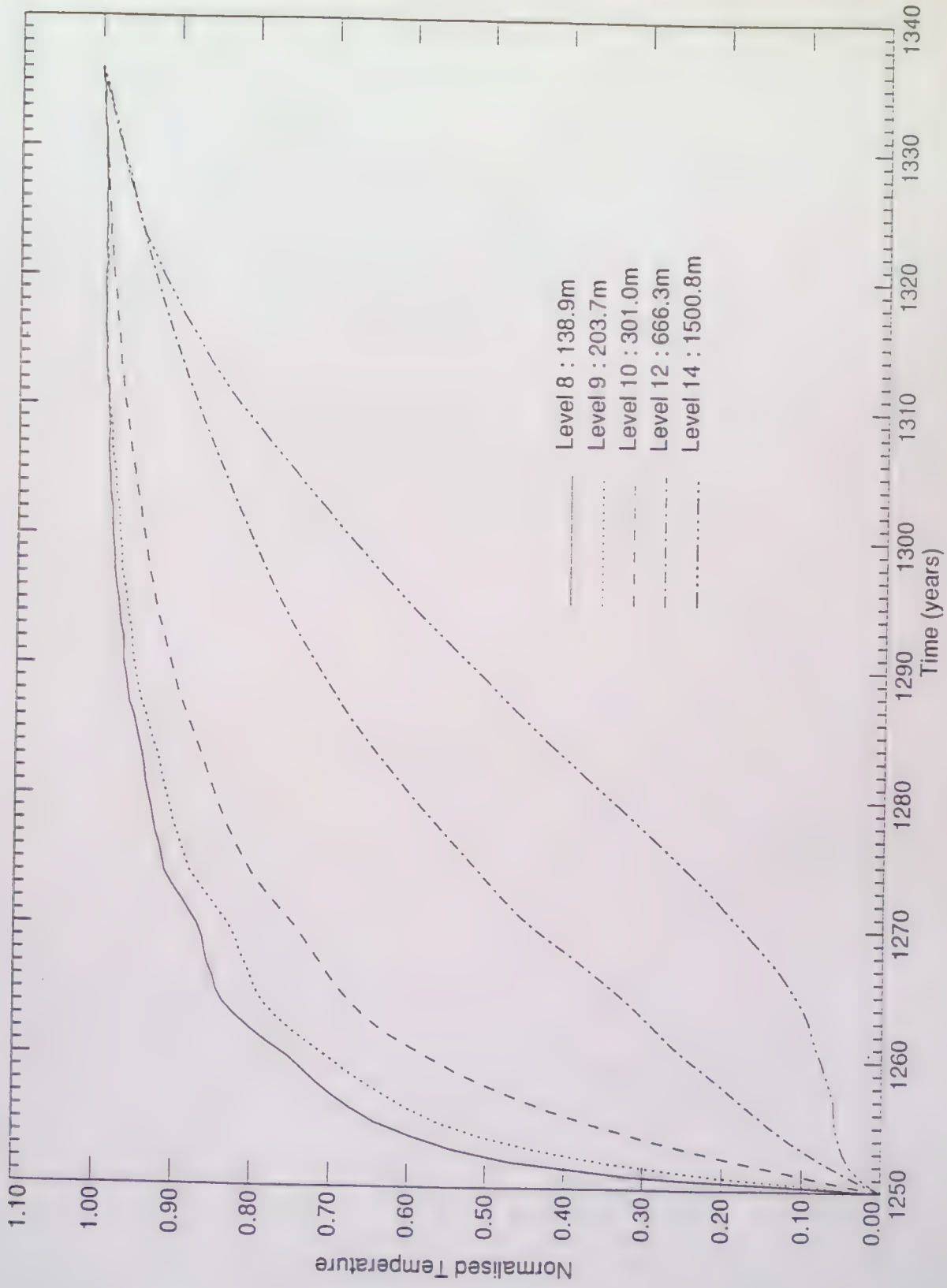

Fig. 1 - Time variation of the normalised globally-averaged temperature during the seasonally-forced period of the run at levels 8,9,10, 12 and 14. Normalisation is calculated as $[T(t) - T_{initial}]/[T_{final} - T_{initial}]$

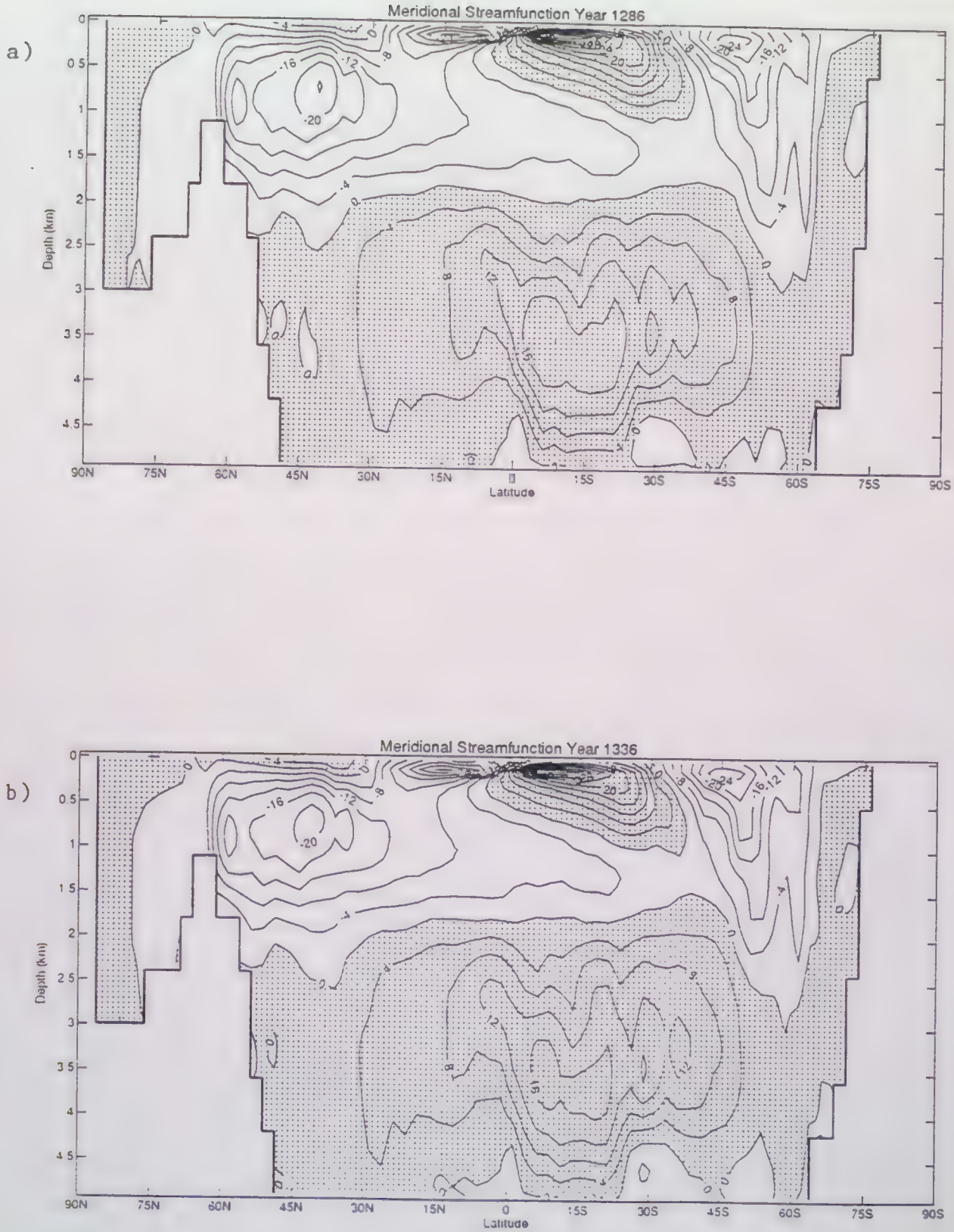

Fig. 2 - Global meridional streamfunction (Sv) at a) the beginning and b) the end of experiment A.

Fig.3 - Model sea surface temperature at the end of the spin-up run for a) January to March, b) April to June, c) July to September and d) October to December. The shaded regions are ice-covered.

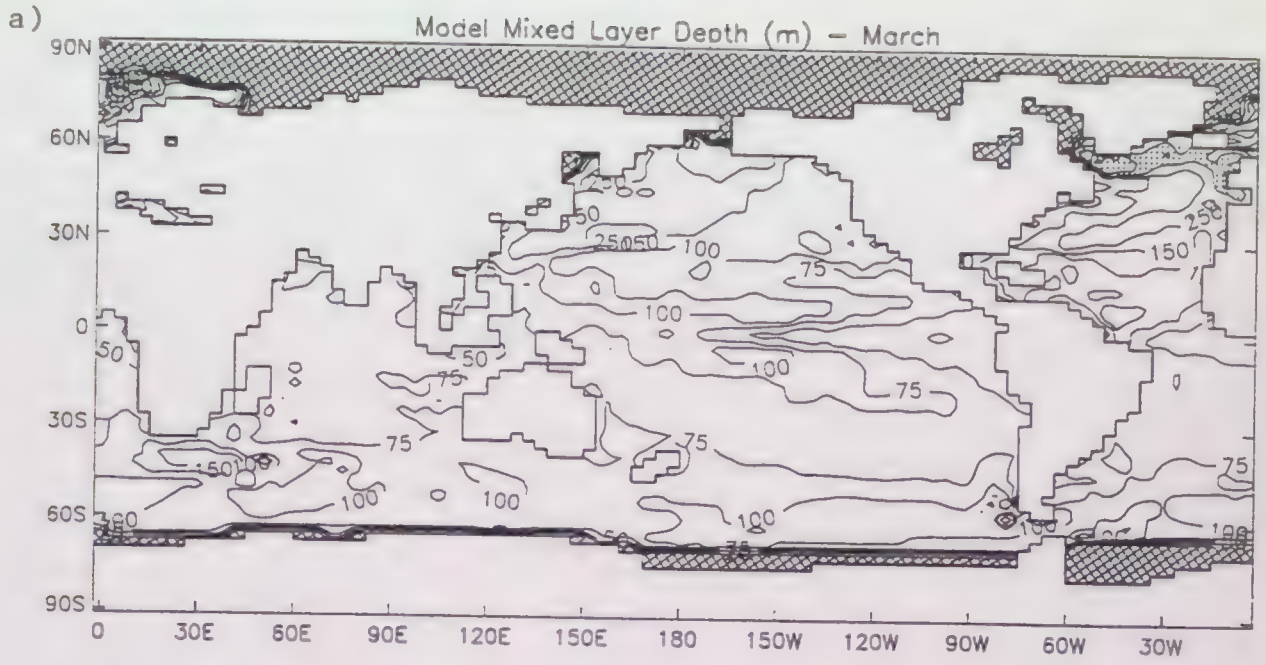

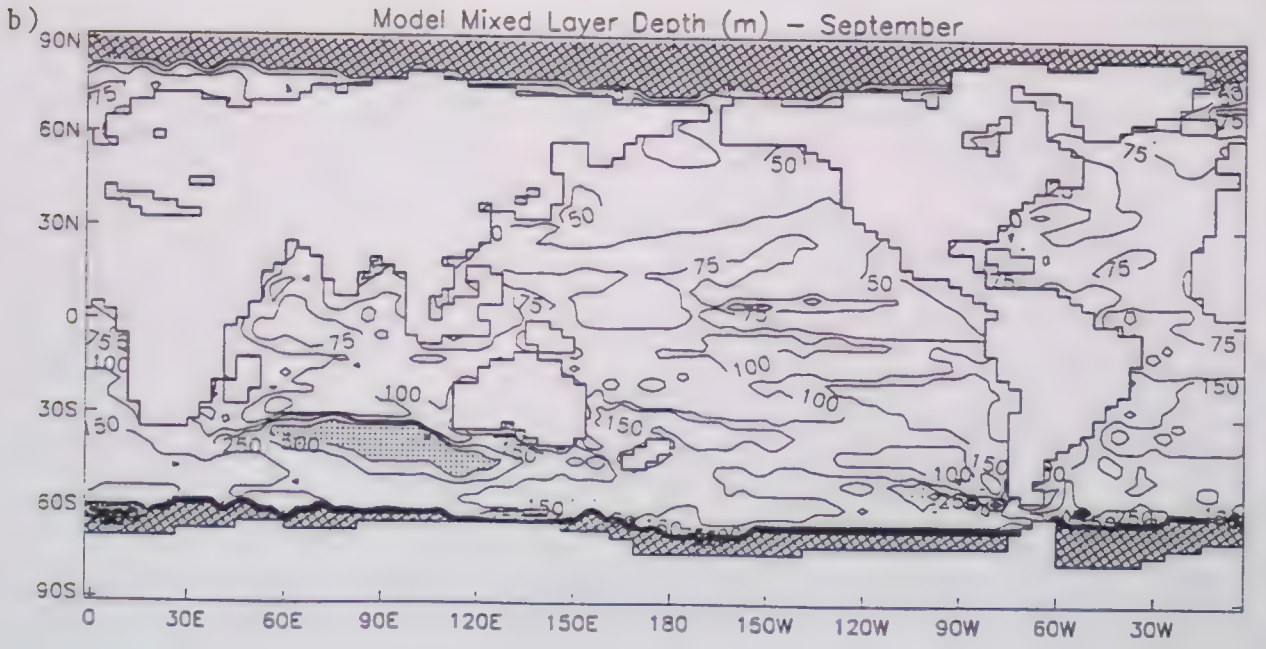

Fig. 4 - Model mixed layer depths at the end of the spin-up run for a) March and b) September. Contours are plotted at 25, 50, 75, 100, 150, 250, 500, 1000, and 2000m. Depths in excess of 500m are stippled. Cross-hatched areas are ice-covered.

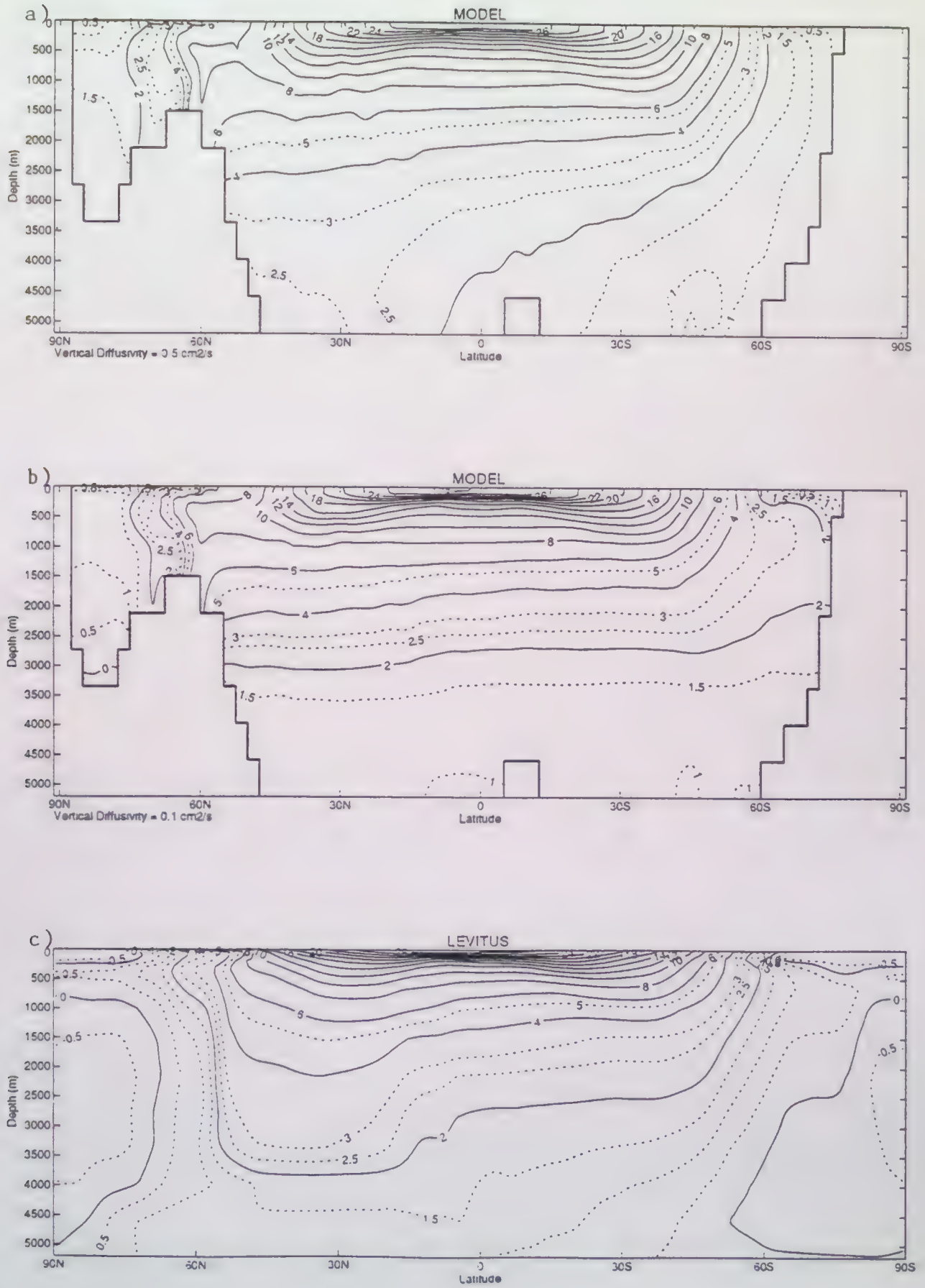

Fig. 5 - Latitude-depth cross-sections of zonal-mean temperature (^{0}C). a) Standard run vertical diffusivity=0.5 cm^2s^{-1}. b) Vertical diffusivity = 0.1 cm^2s^{-1}. c) Observed values from Levitus (1982).

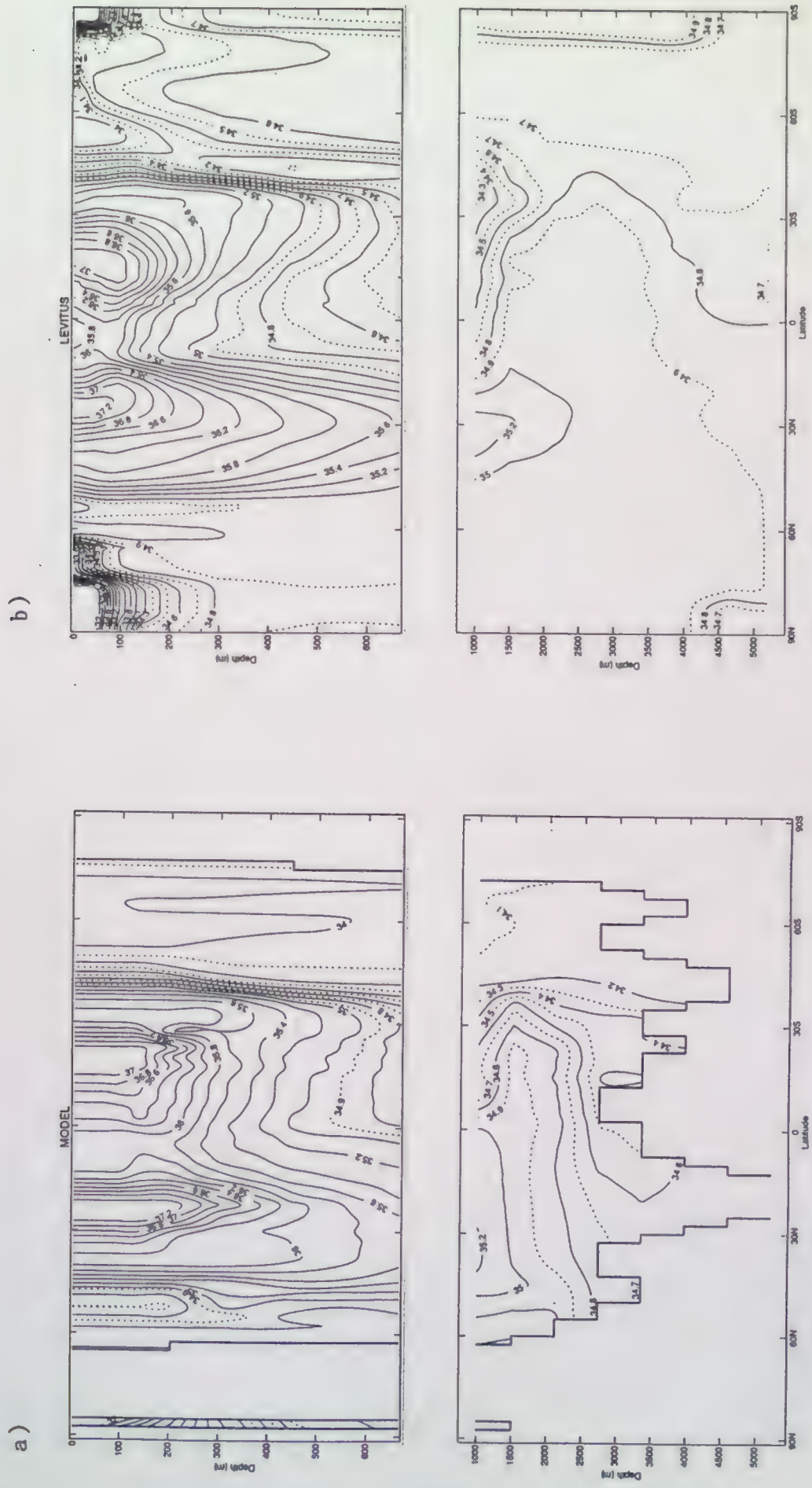

Fig. 6 - Latitude-depth cross-section of Atlantic salinity (psu) for a) Model (standard run), and b) observations (Levitus).

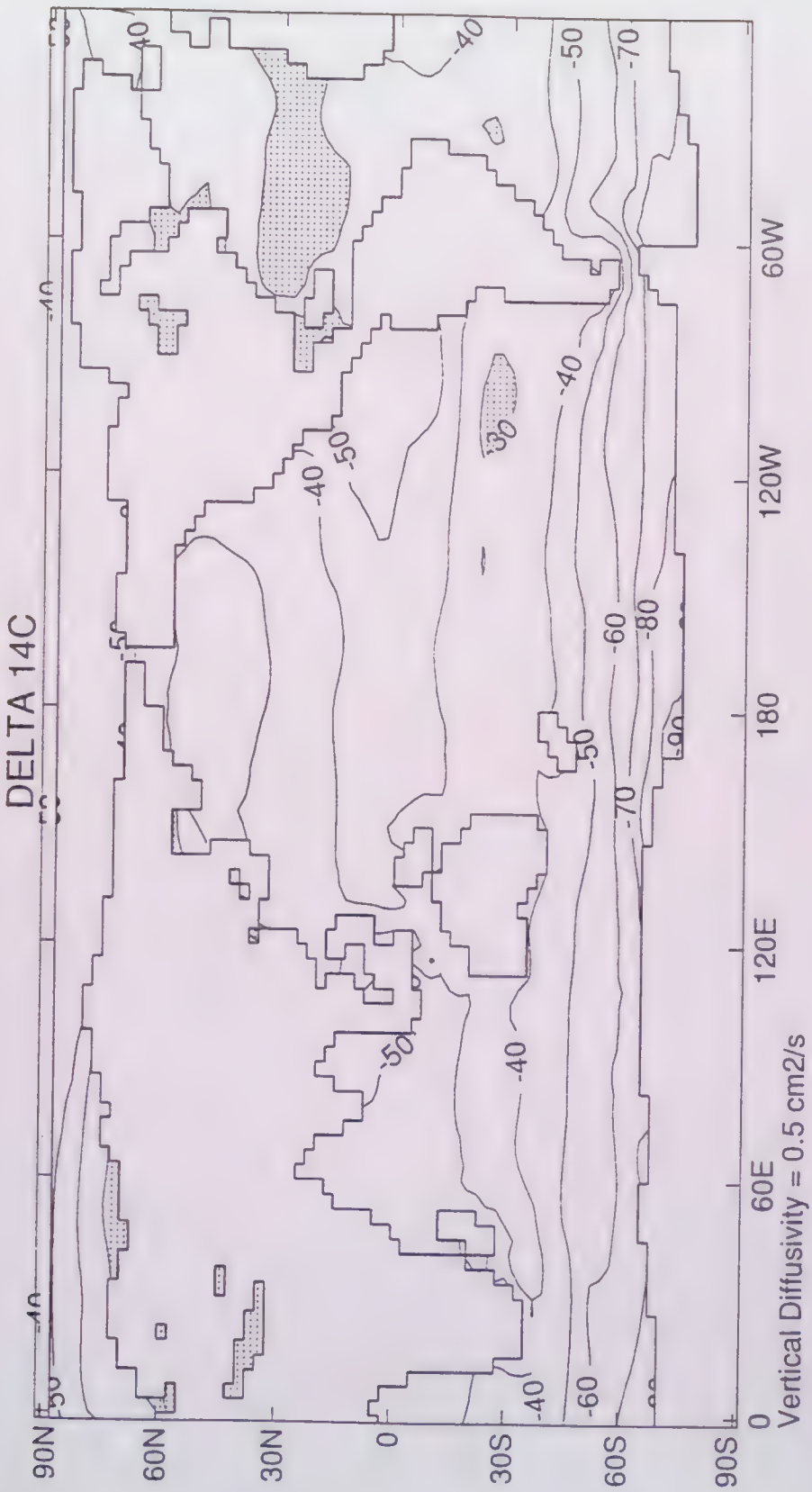

Fig. 7 - Predicted $\Delta^{14}C$ (per mil) at the surface from the standard run of the model. Values above -30 ‰ are shaded.

a)

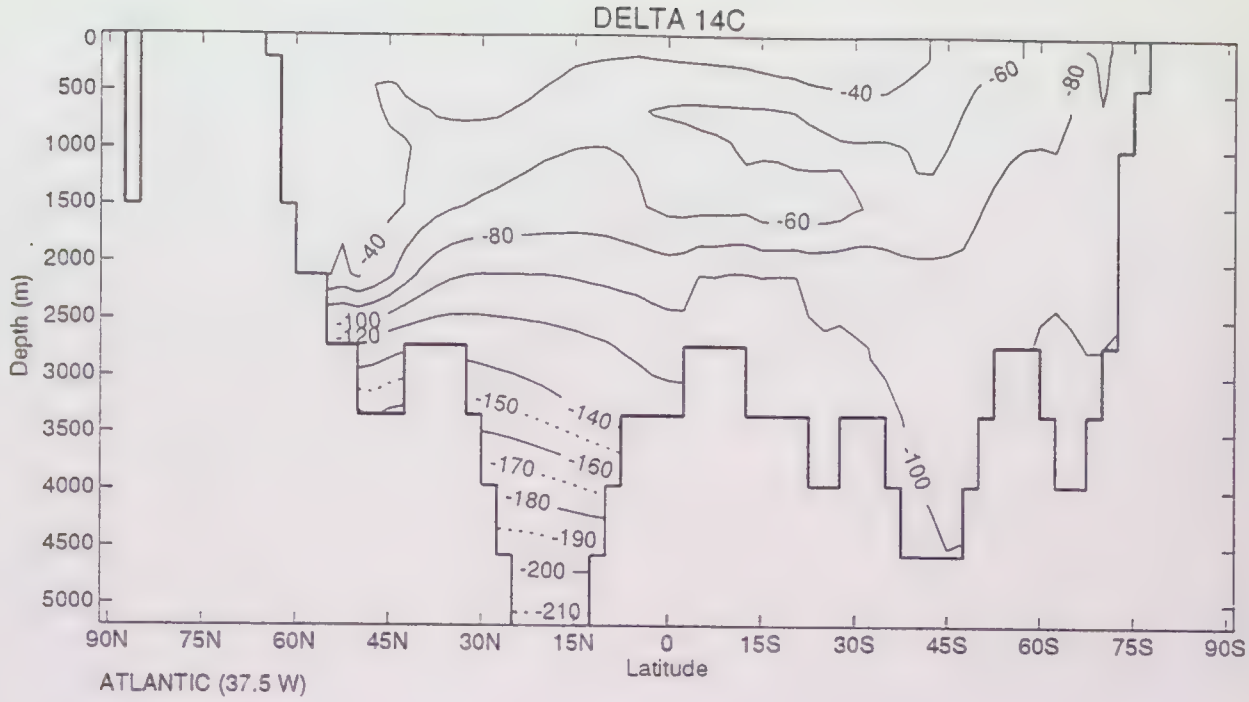

b)

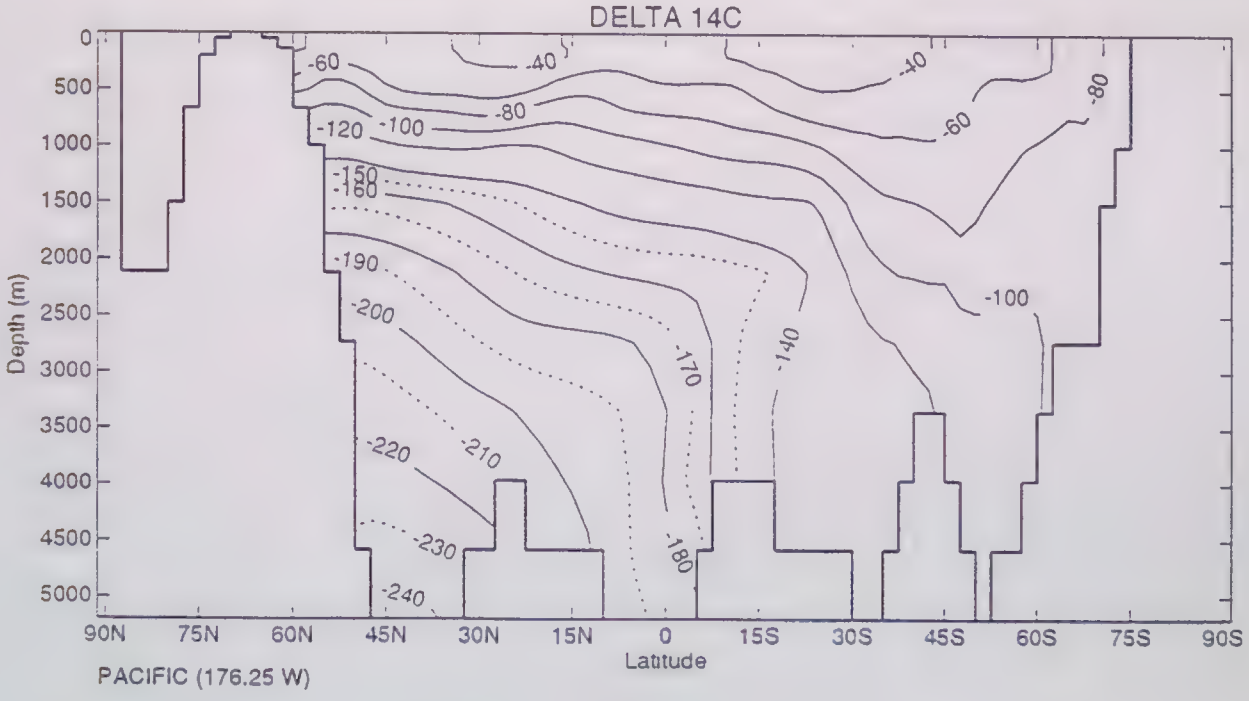

Fig 8 - Predicted latitude-depth cross-sections of $\Delta^{14}C$ (per mil) from the standard run through a) the Atlantic at 37.5 ^{0}W, and b) the Pacific at 176.25 ^{0}W.

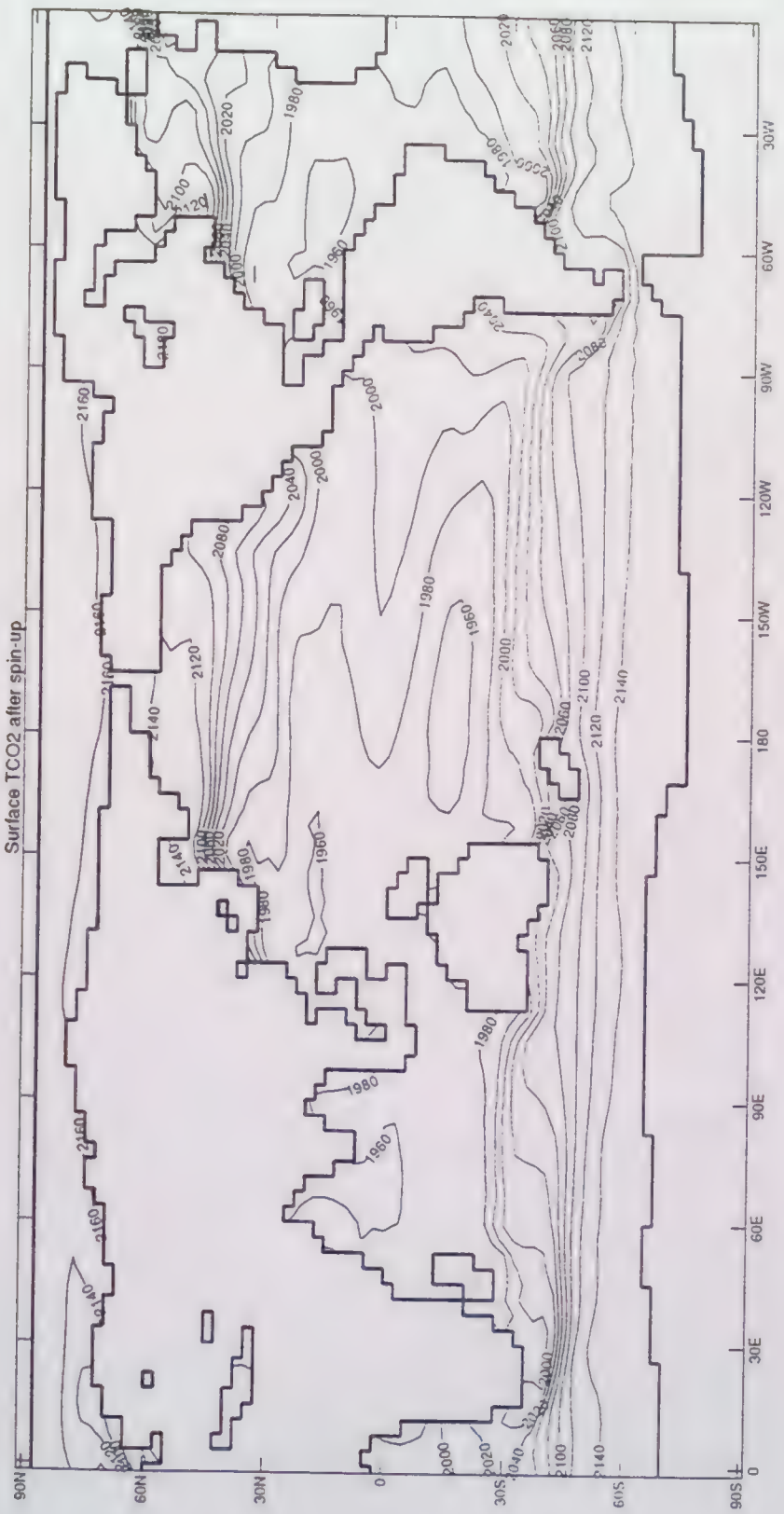

Fig 9 - Annual mean surface TCO2 (in uMoles kg^{-1}) at the end of the spin-up run.

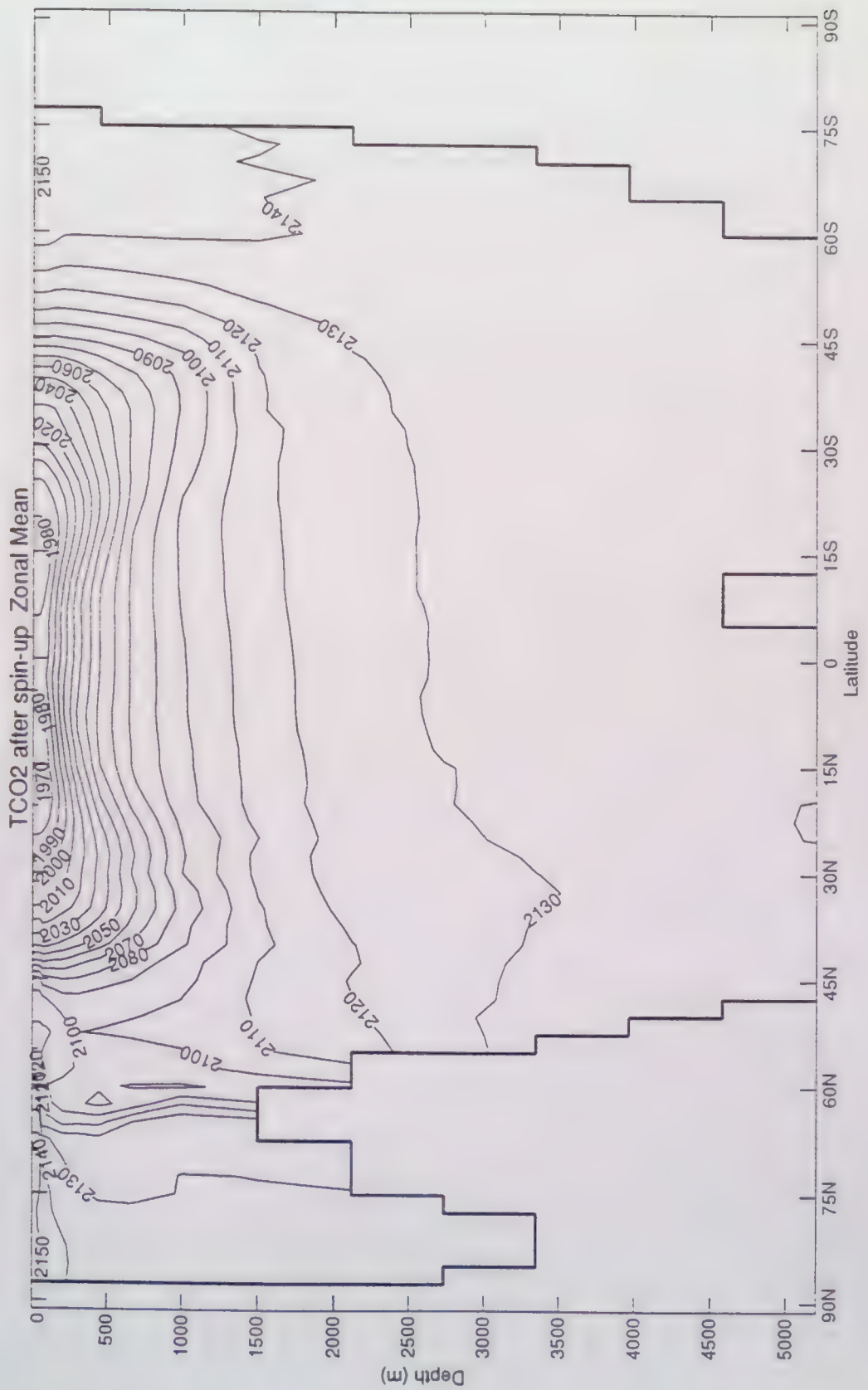

Fig 10 - Zonally-averaged meridional section of TCO2 (in uMoles kg ^{1}) at the end of the spin-up run.

a)

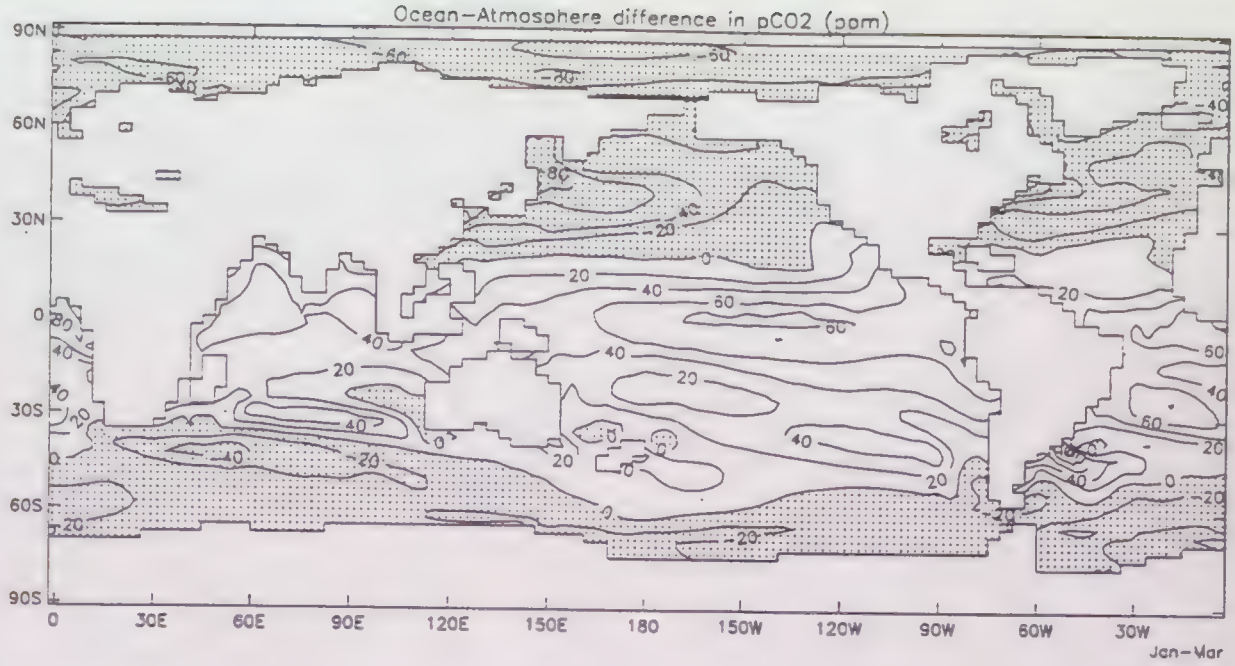

b)

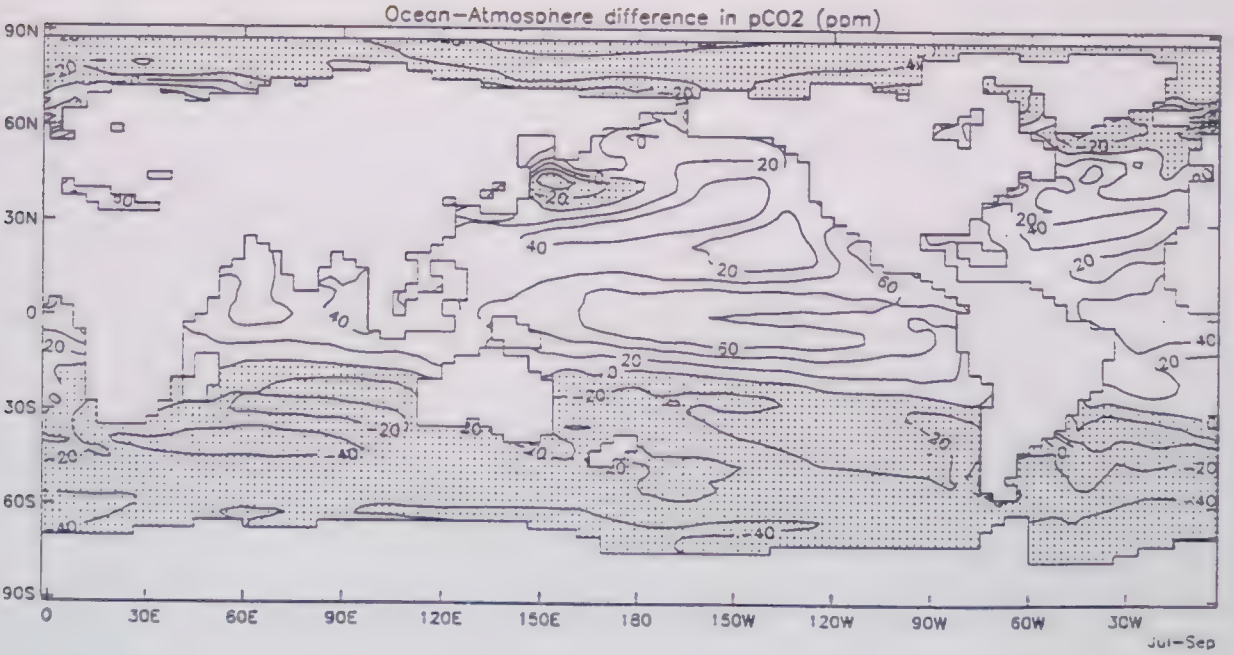

Fig 11 - Model ΔpCO_2 in ppm at the end of the spin-up run for a) January to March; and b) July to September. Negative values (representing gas flux into the sea) are shaded.

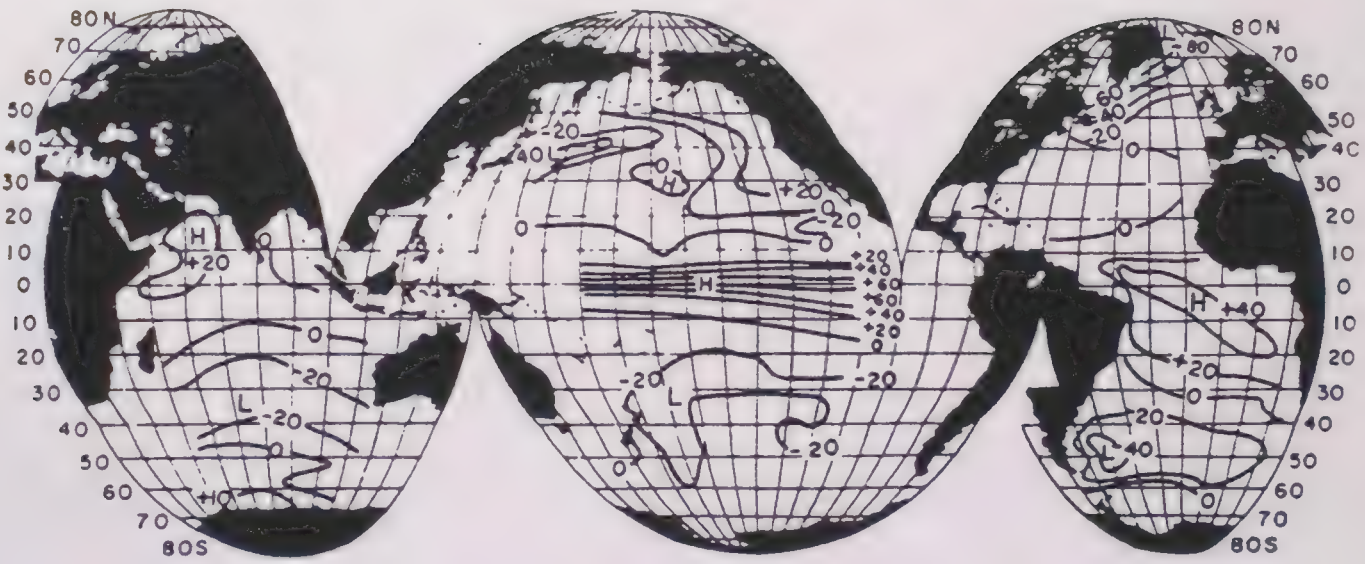

Fig 12 - ΔpCO_2 observed during the Geosecs program. Summer conditions are shown in both hemispheres.

(From Takahashi and Azevado, 1982)

a)

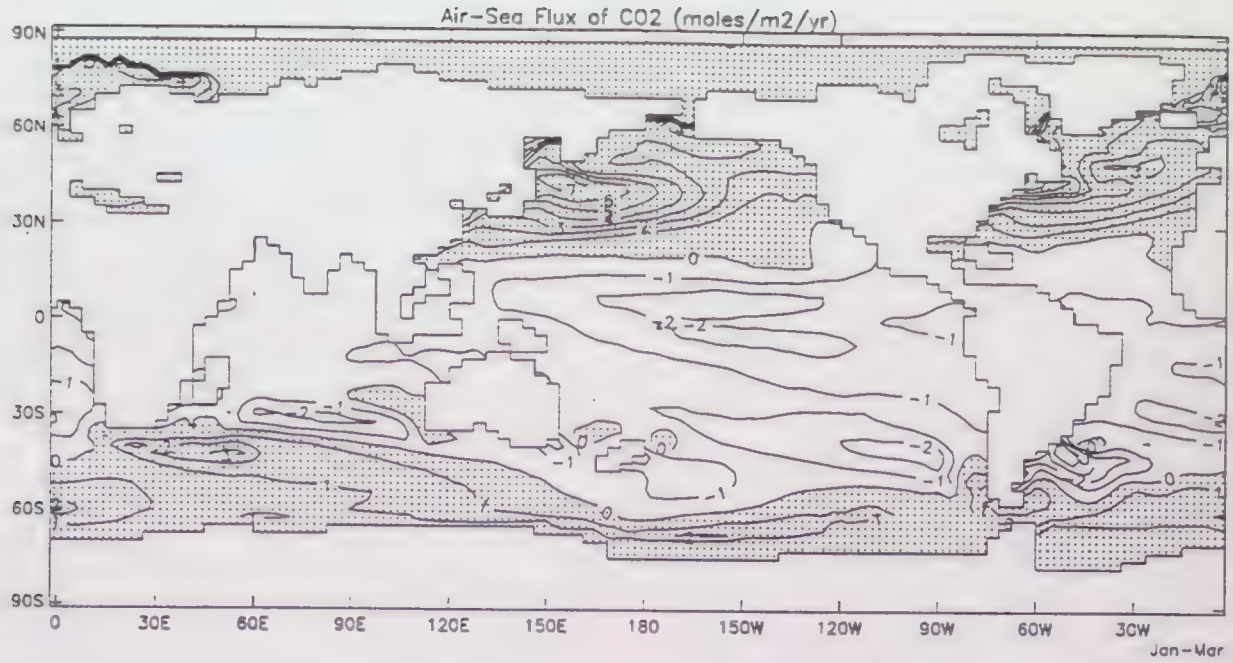

b)

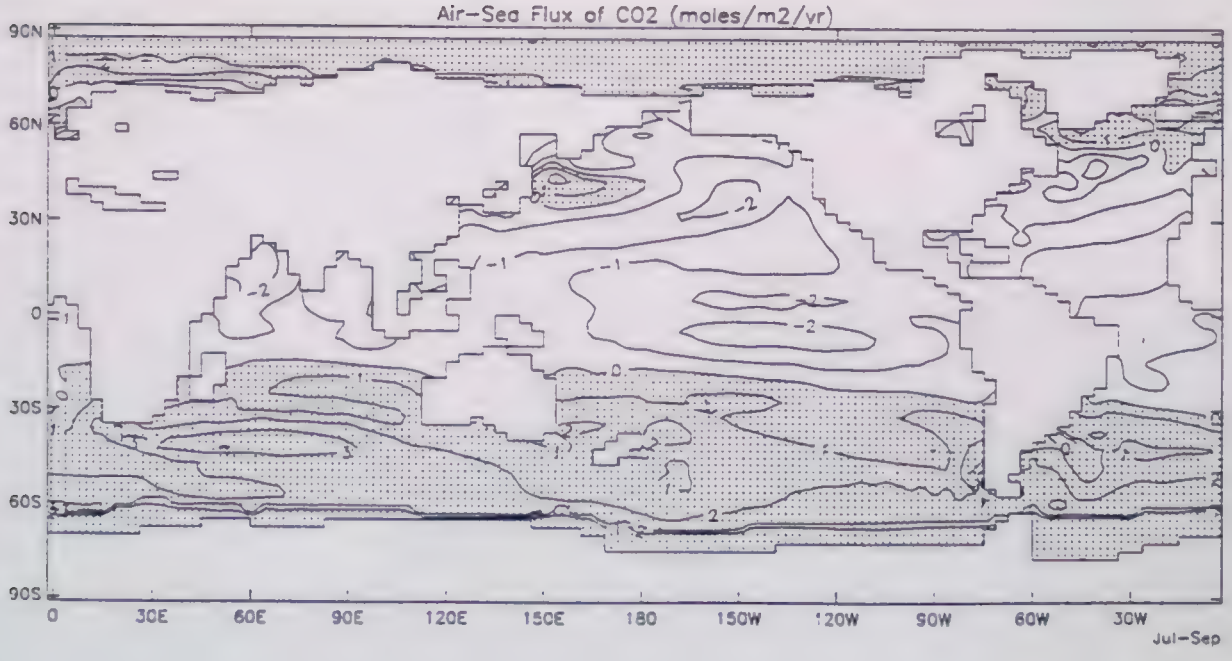

Fig 13 - Atmosphere - ocean gas flux in mol m^{-2} yr^{-1} during the latter stages of the spin-up. a) January to March. b) July to September. Positive values, representing flux into the ocean, are shaded.

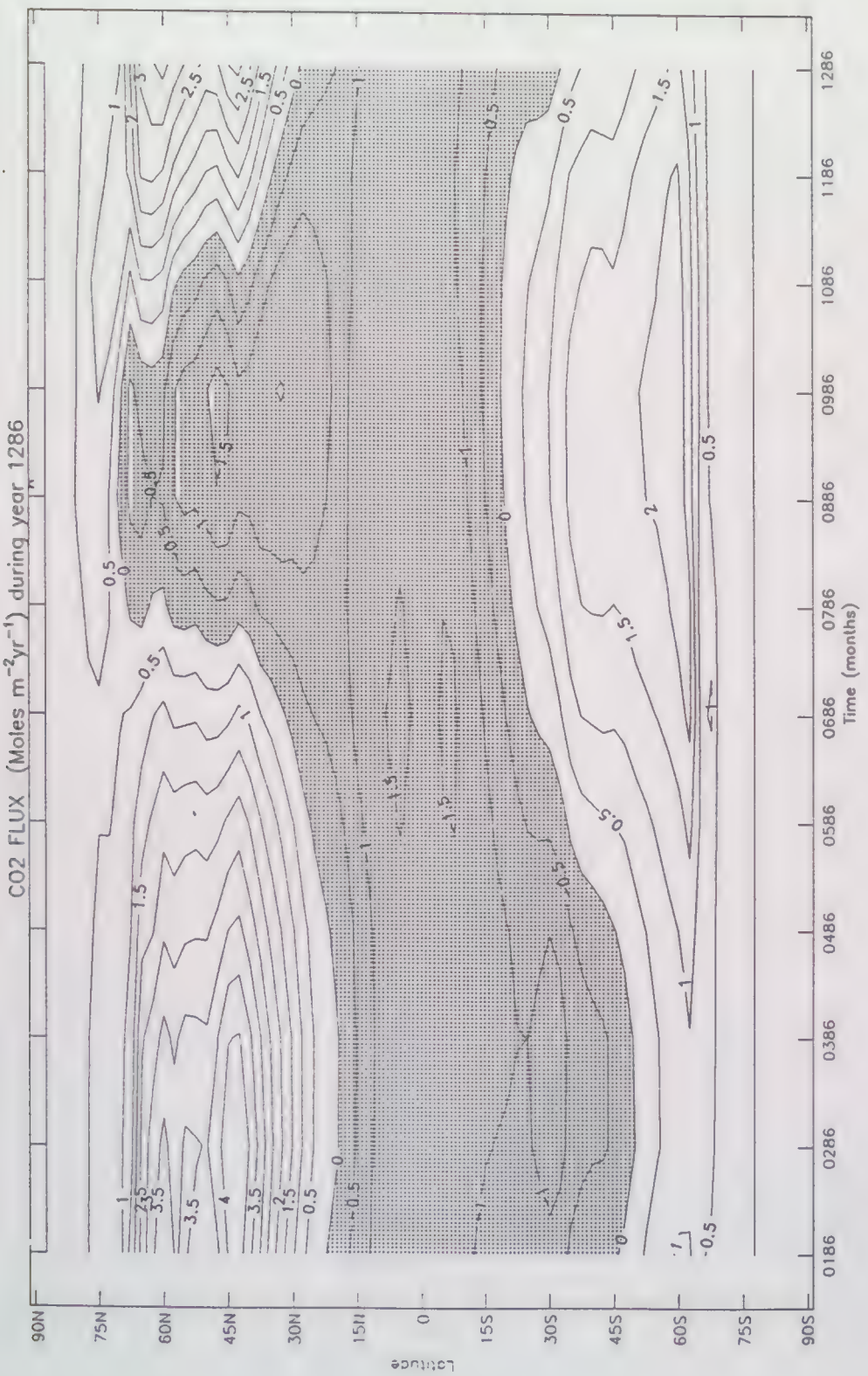

Fig 14 - Time-latitude plot of the zonal mean CO_2 flux in mol m^{-2} yr^{-1} during the final year of the spin-up.

Negative values, representing flux out of the ocean, are shaded

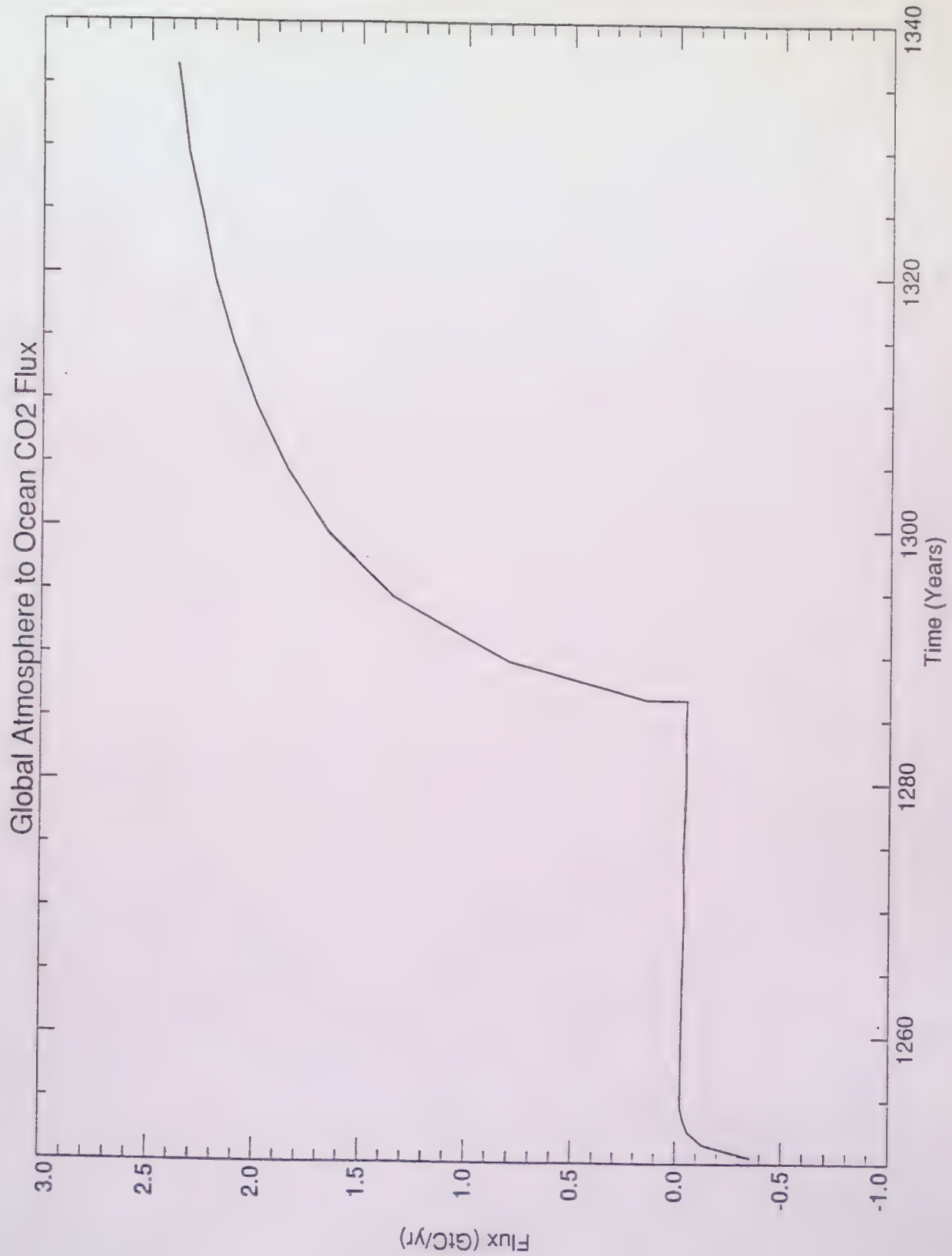

Fig 15 - Time series of the global net exchange of carbon in GtC yr^{-1} between atmosphere and ocean during stage III of the spin-up and experiment A - the seasonally forced part of the integration. After year 1286 CO_2 was added to the atmosphere at a constant rate of 5.4 GtC yr^{-1}. The seasonal cycle has been suppressed in the figure by plotting annual mean fluxes.

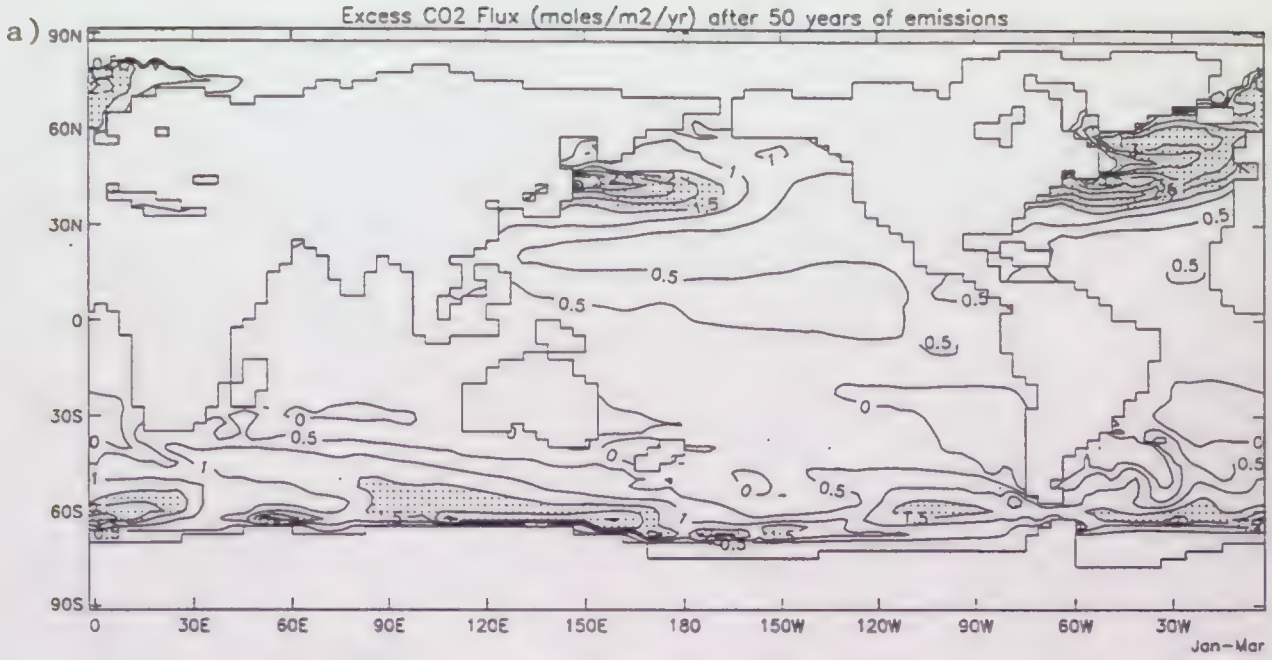

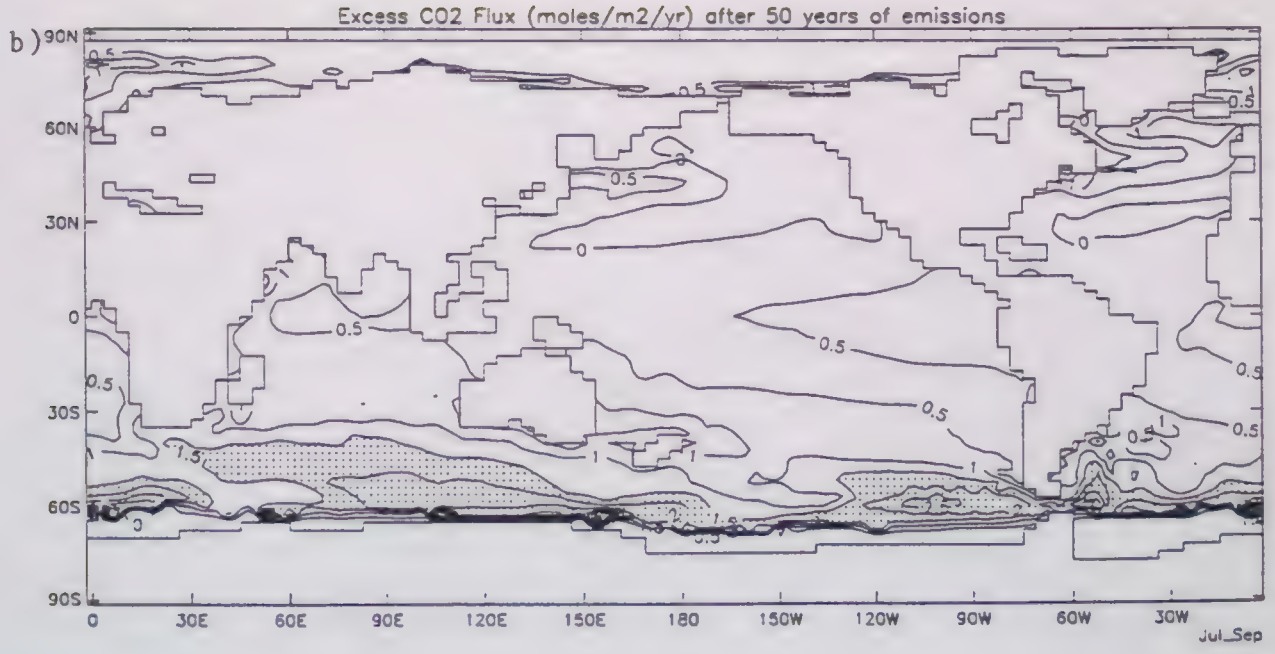

Fig 16 - Atmosphere to ocean flux of excess CO_2 in mol m^{-2} yr^{-1} after 50 years of experiment A for a) January to March, and b) July to September. Fluxes in excess of 1.5 mol m^{-2} yr^{-1} are shaded. Excess CO_2 flux was obtained by plotting the difference between the fluxes during experiment A and those at the end of the spin-up run.

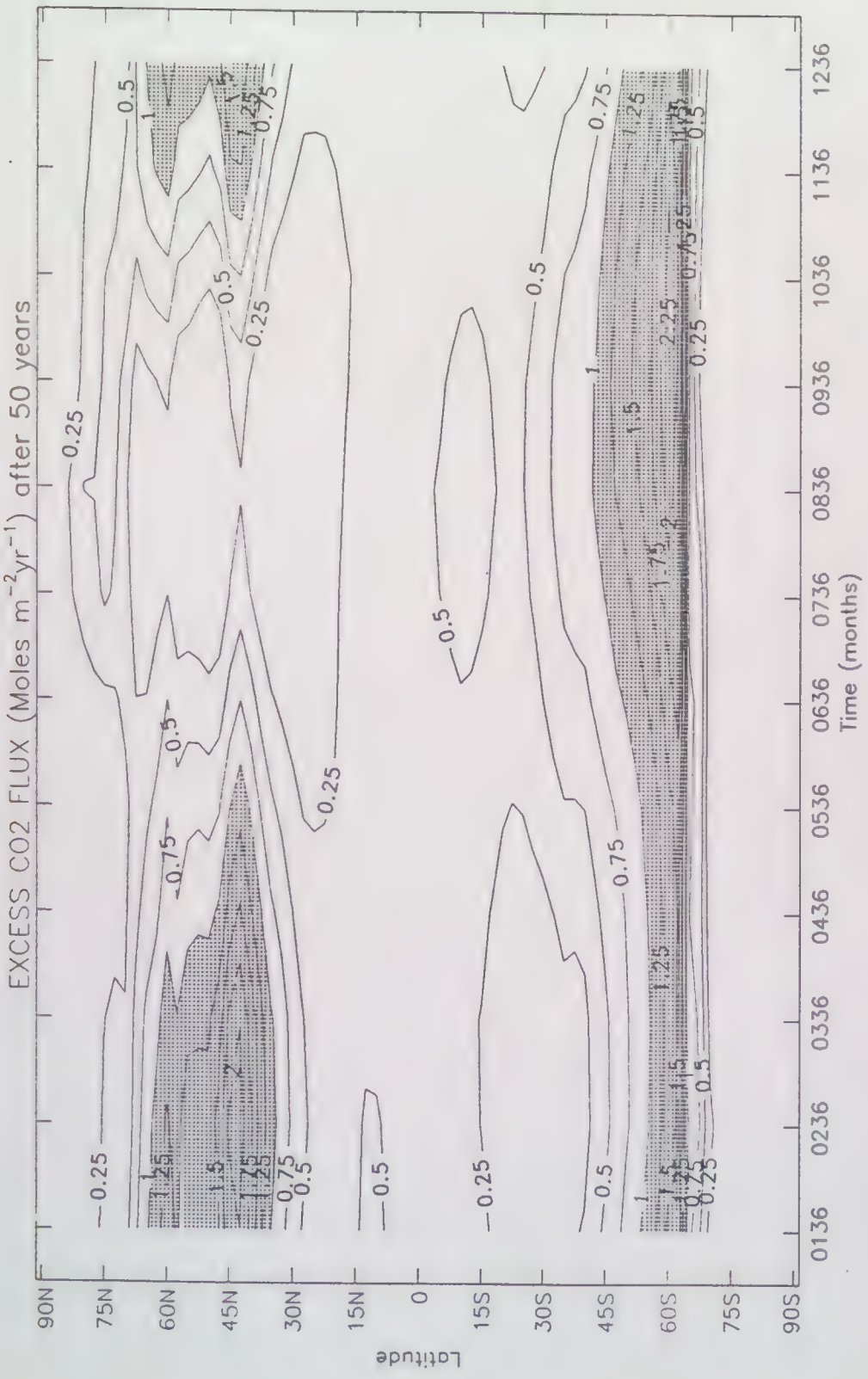

Fig 17 - Time-latitude plot of the zonal mean excess CO_2 flux in mol m^{-2} yr^{-1} after 50 years of experiment A. Fluxes in excess of 1 mol m^{-2} yr^{-1} are shaded. Excess CO_2 flux was obtained by plotting the difference between the fluxes during experiment A and those at the end of the spin-up run.

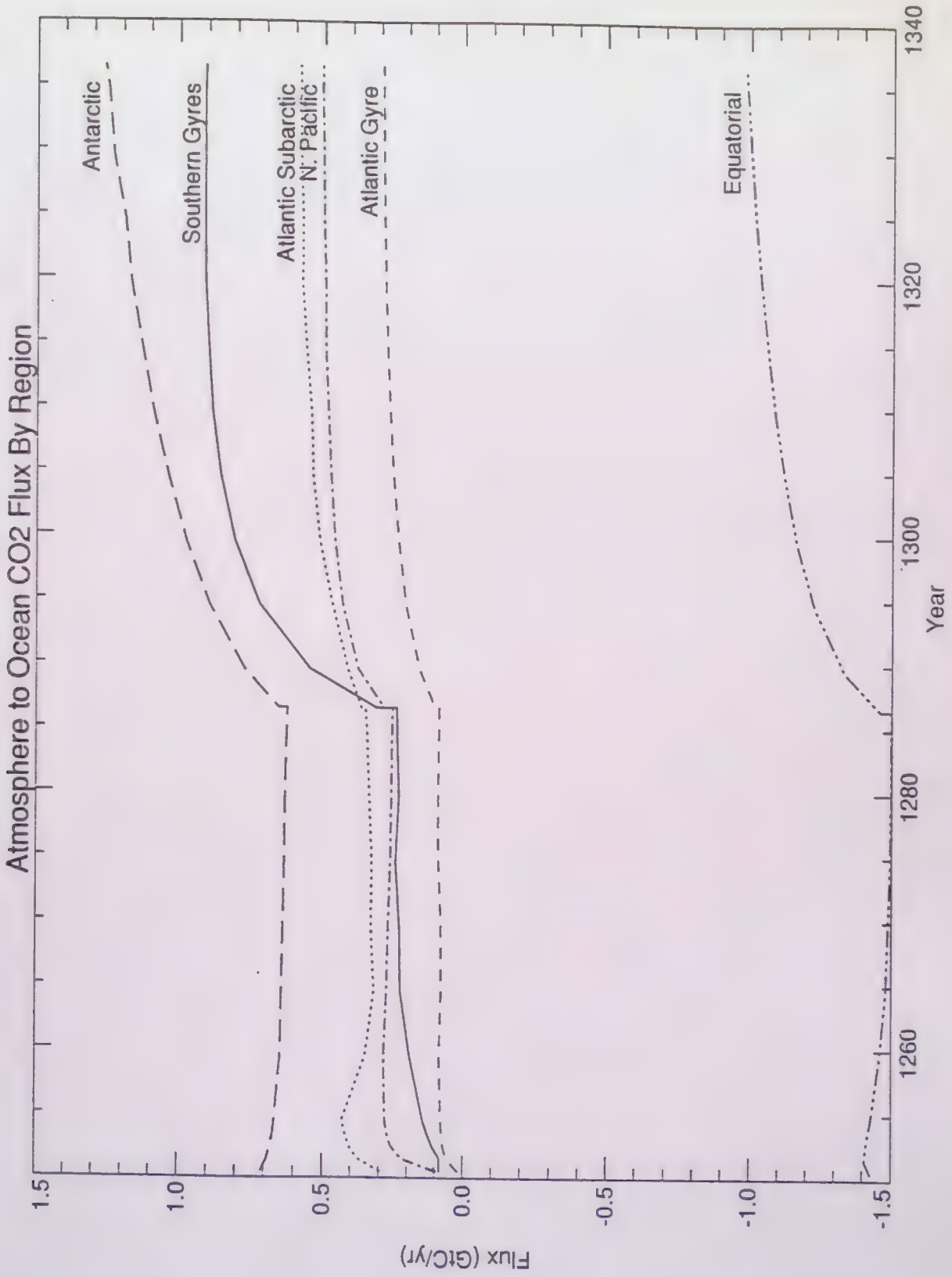

Fig 18 - Time - series of atmosphere to ocean CO_2 flux (in GtC yr^{-1}) for each of the regions defined in Table 3 for stage III of the spin-up and experiment A - the seasonally forced part of the integration. The seasonal cycle has been suppressed in the figure by plotting annual mean fluxes.

a)

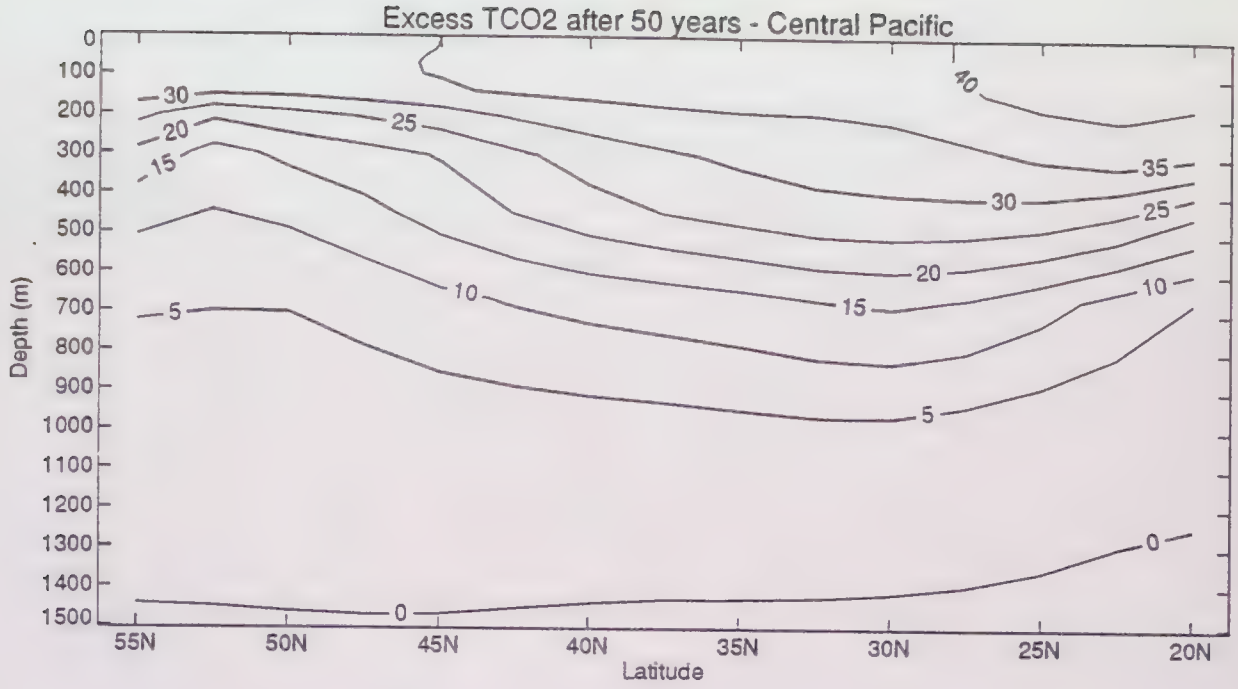

b)

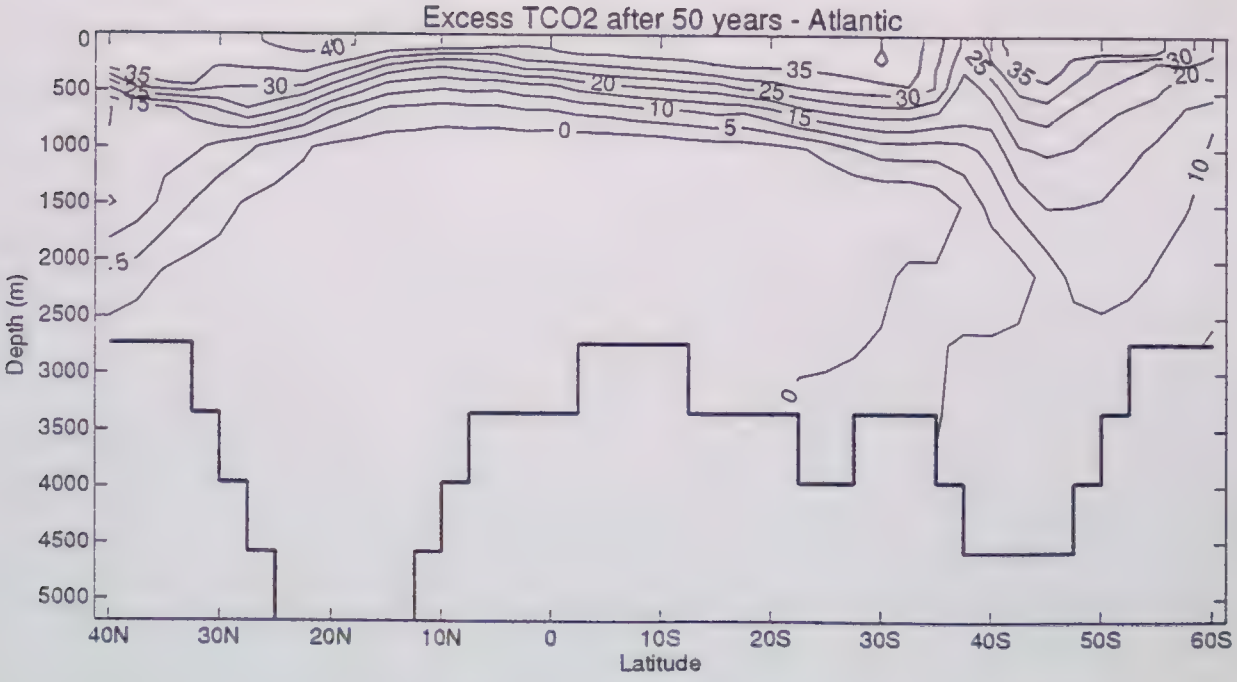

Fig 19 - Meridional sections of excess TCO2 in μmol kg^{-1} after 50 years of experiment A for a) the North Pacific ocean, and b) the Atlantic ocean at 20* W. Excess TCO2 is obtained by plotting the difference between TCO2 during experiment A, and at the end of the spin-up run.

a)

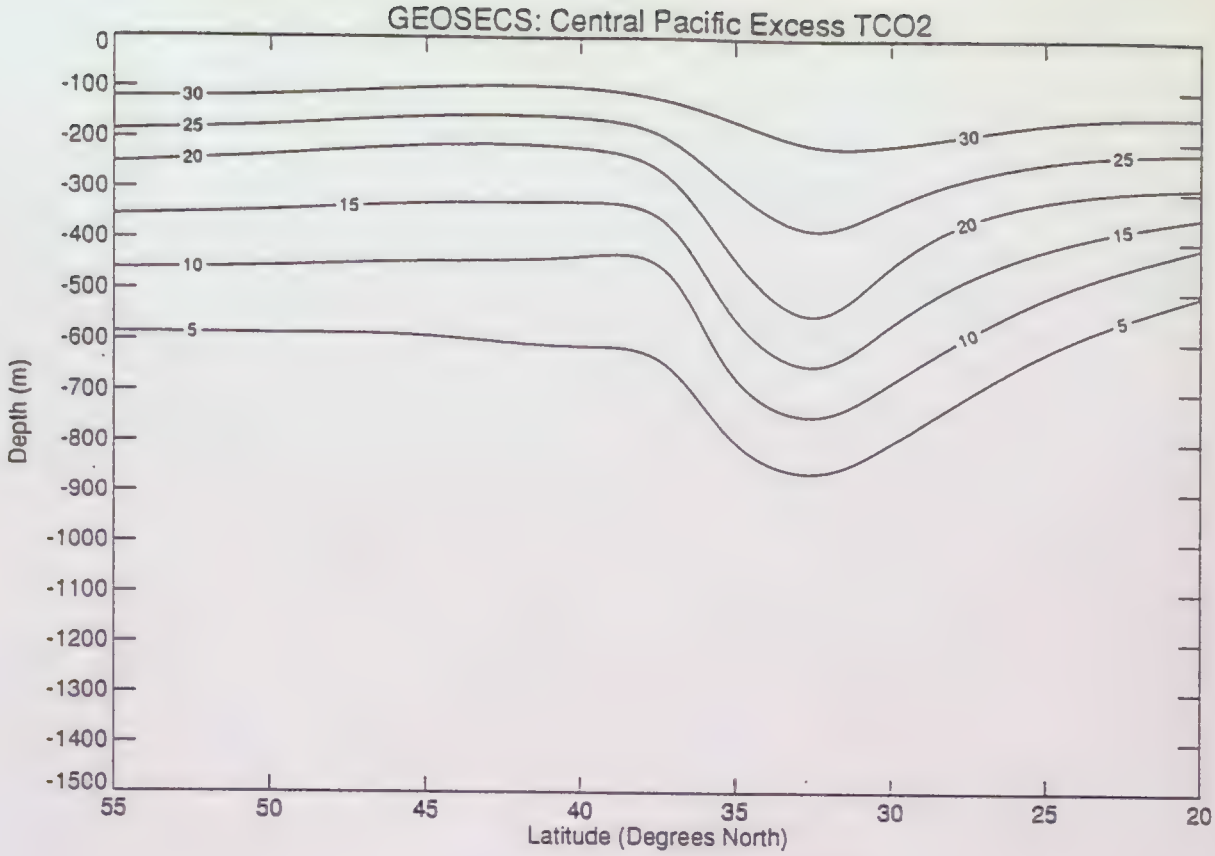

b)

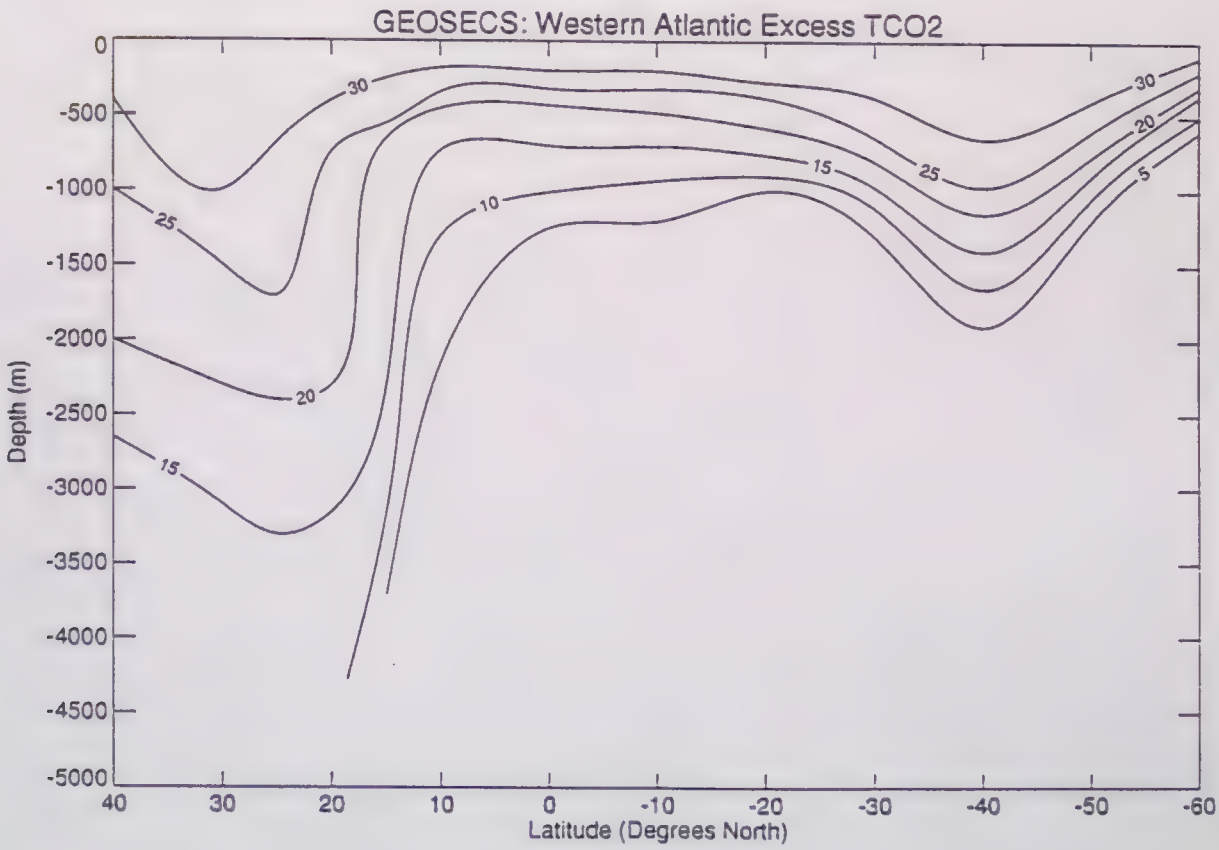

Fig 20 - Observationally-based estimates of excess TCO2 from the GEOSECS expedition for a) the North Pacific ocean (from Chen, 1982b), and b) the western Atlantic ocean (from Chen, 1982a)

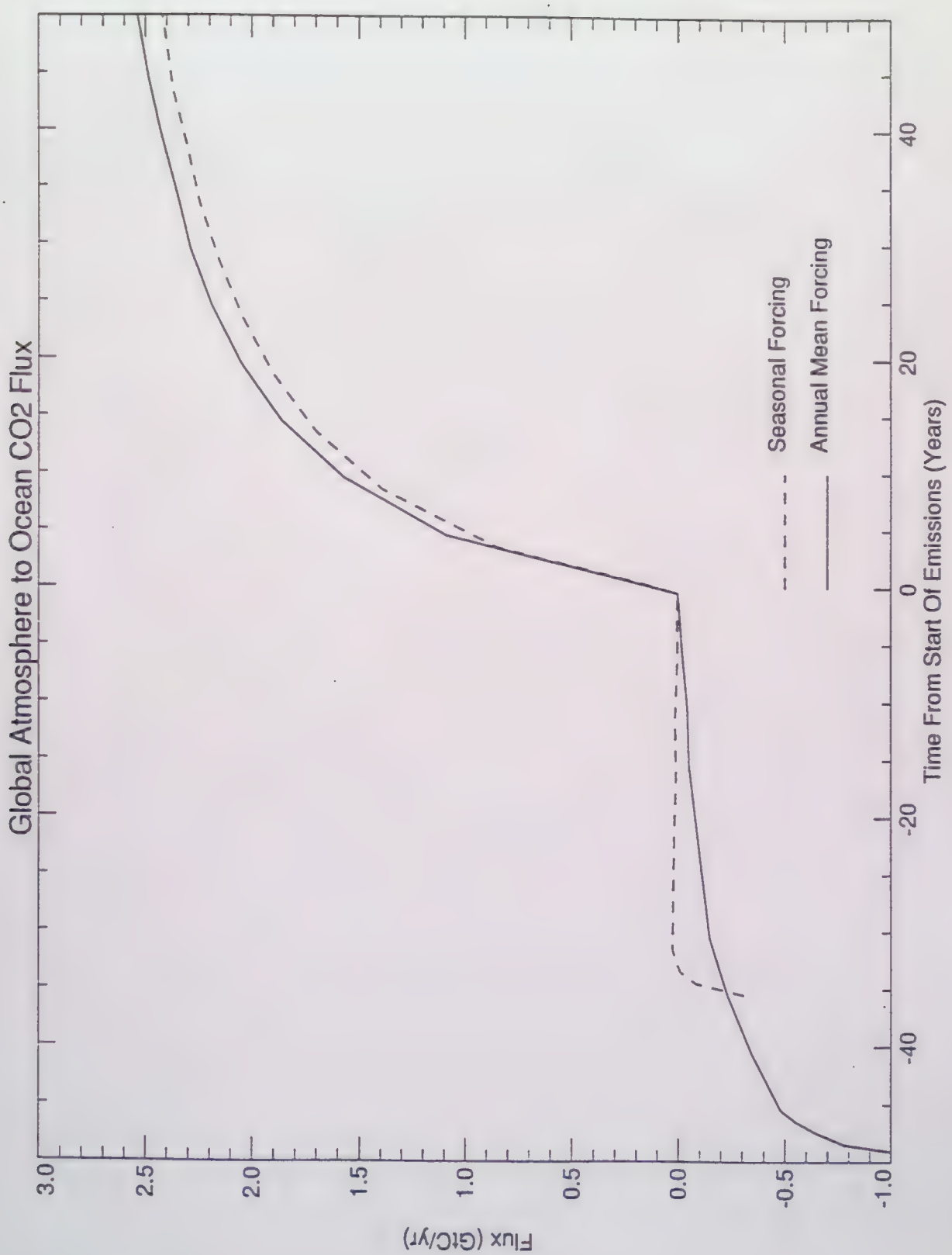

Fig 21 - Comparison between global atmosphere to ocean CO_2 flux under conditions of annual-mean forcing and seasonal forcing. Each curve has been plotted so that it starts from an initial flux of zero at the time emissions to the atmosphere started.

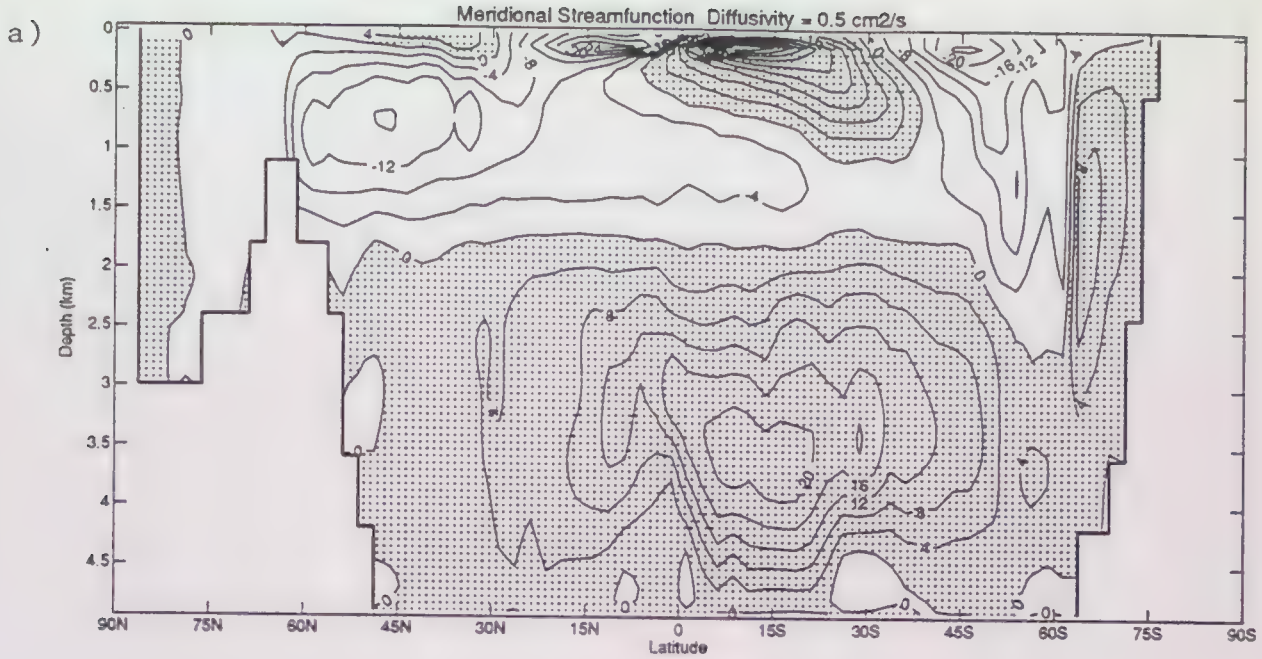

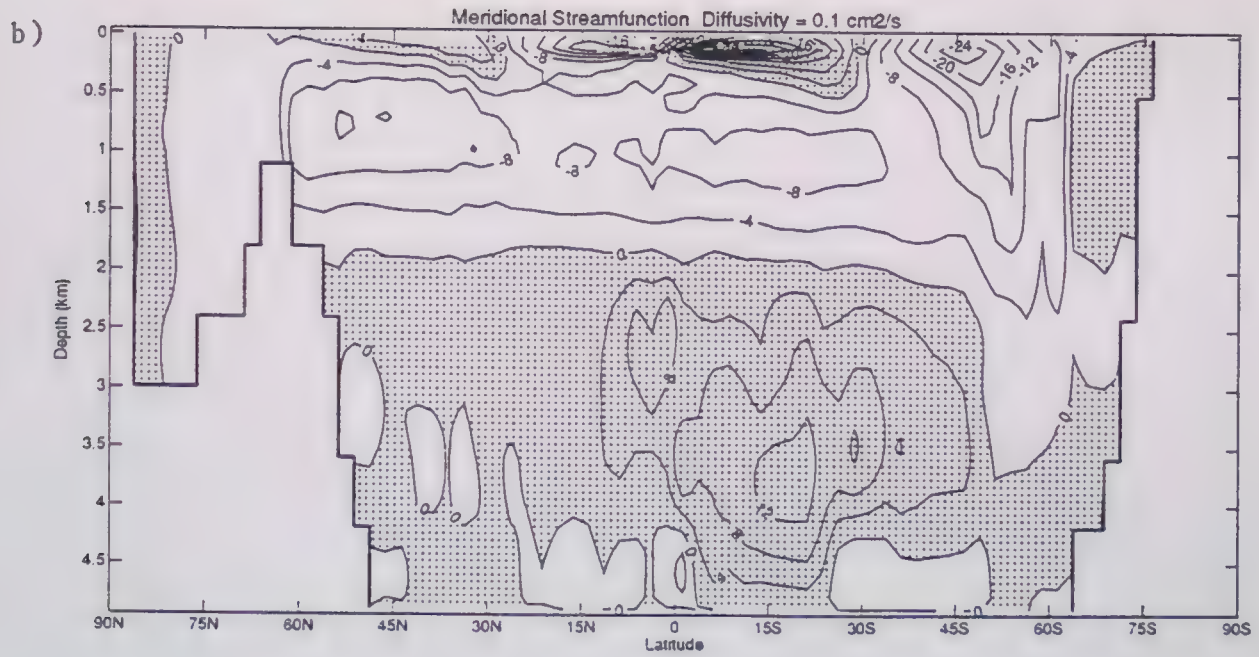

Fig 22 - Global meridional overturning circulation for annual-mean forcing with background vertical diffusivities of a) 0.5 $cm^2 s^{-1}$, and b) 0.1 $cm^2 s^{-1}$. Clockwise circulations are shaded.

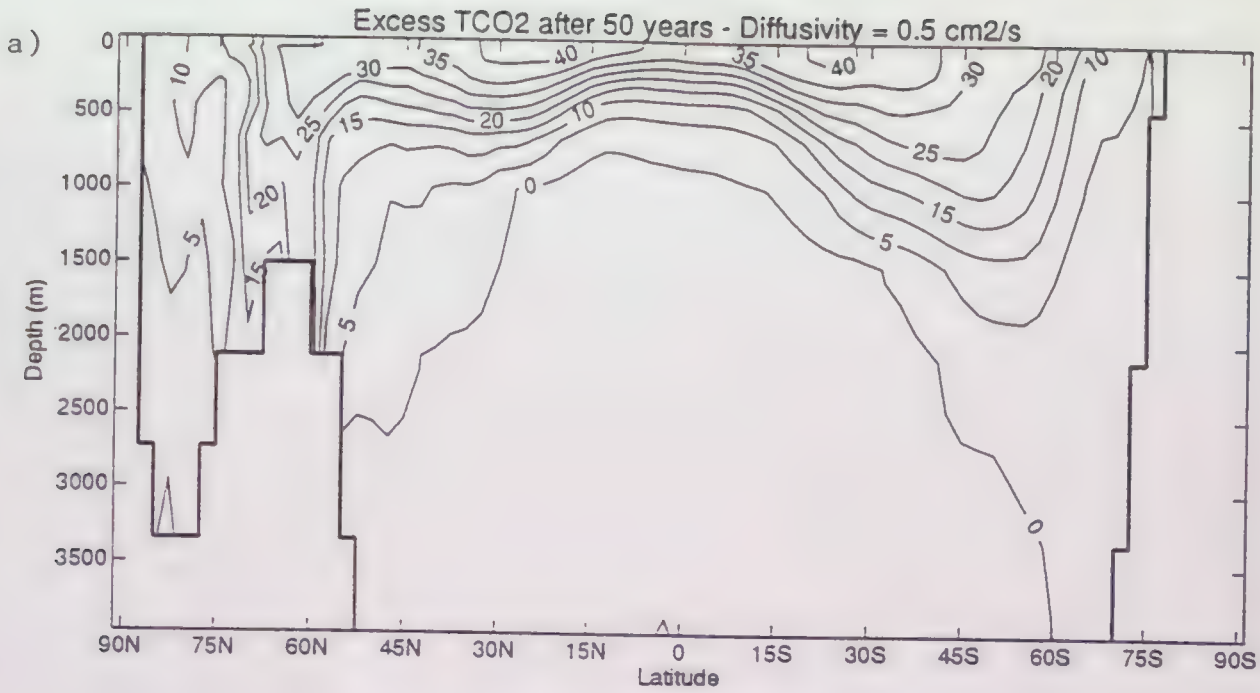

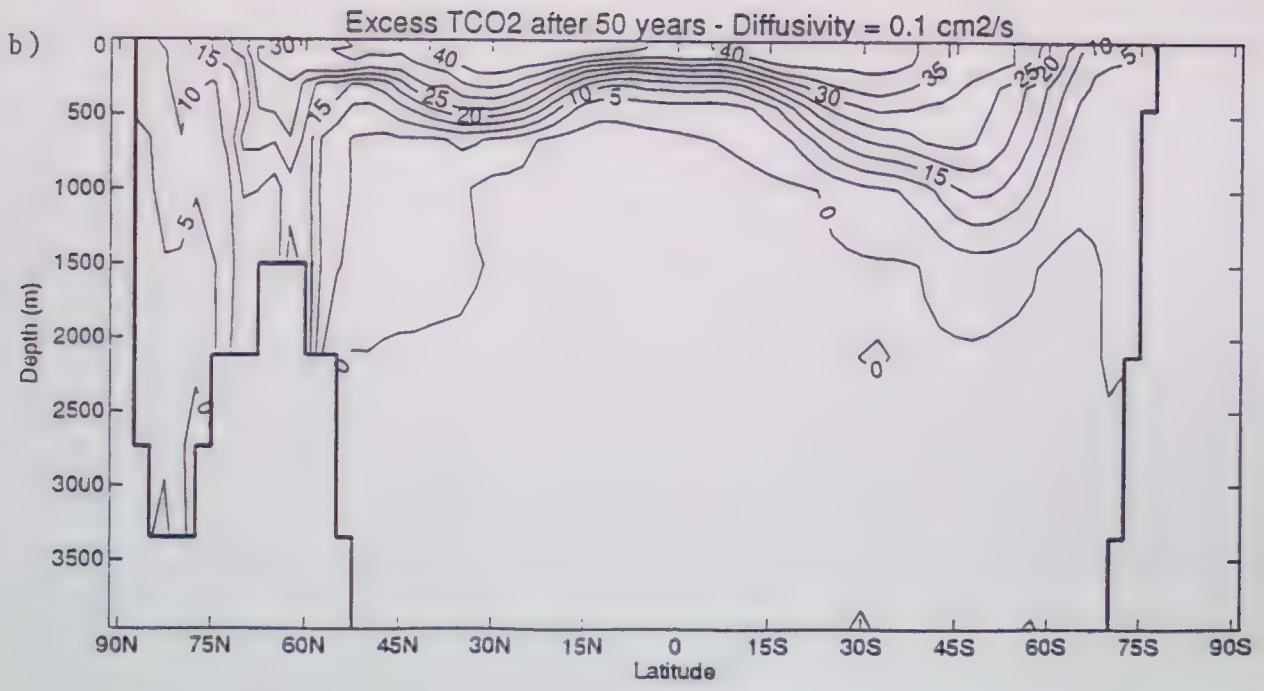

Fig 23 - Meridional sections of zonally-averaged excess TCO2 in µmol kg^{-1} after 50 years of atmospheric emissions for background vertical diffusivities of a) 0.5 $cm^2 s^{-1}$, and b) 0.1 $cm^2 s^{-1}$.

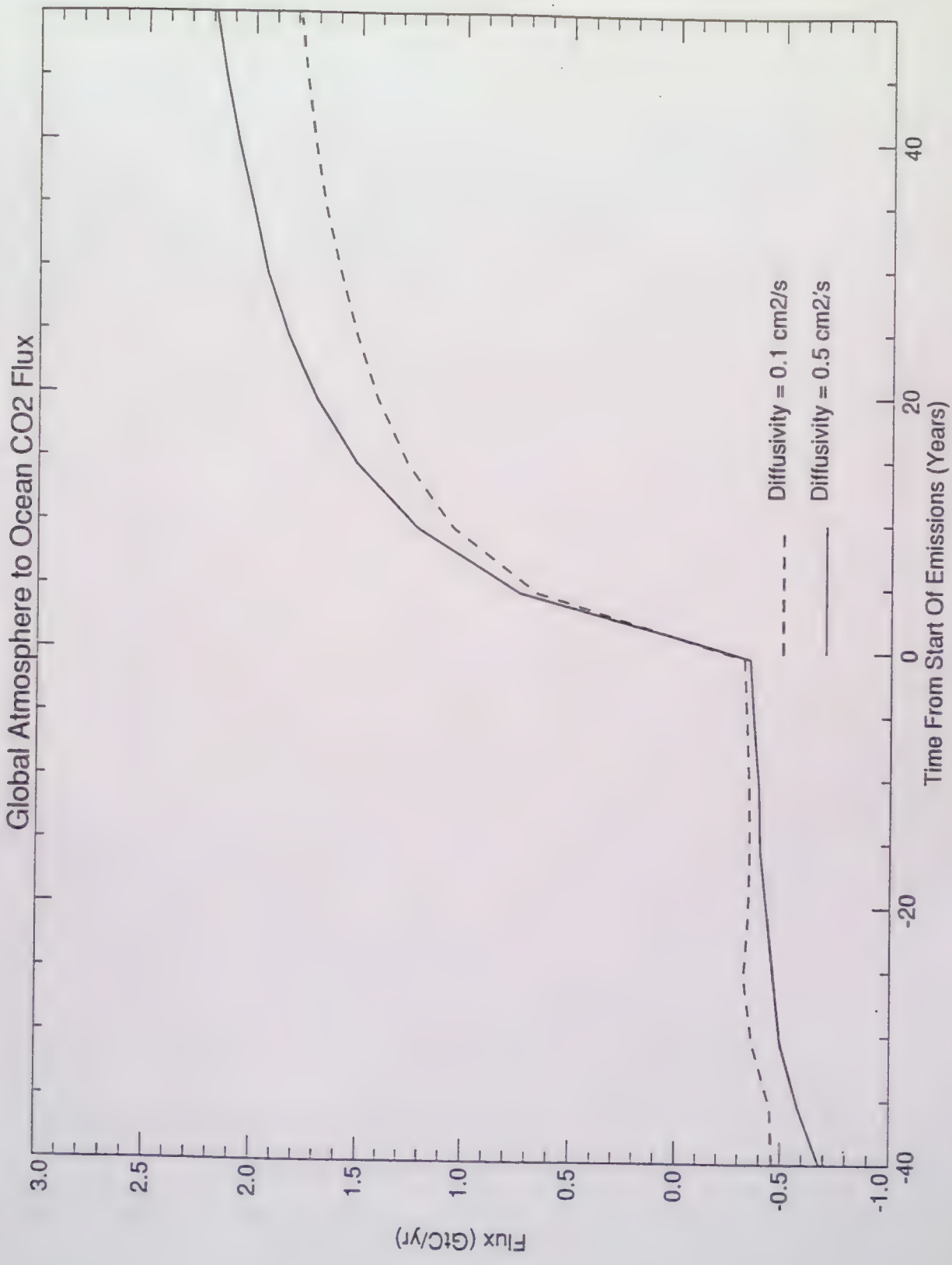

Fig 24 - Comparison between global atmosphere to ocean CO_2 flux for background vertical diffusivities of 0.5 $cm^2\ s^{-1}$ and 0.1 $cm^2\ s^{-1}$.

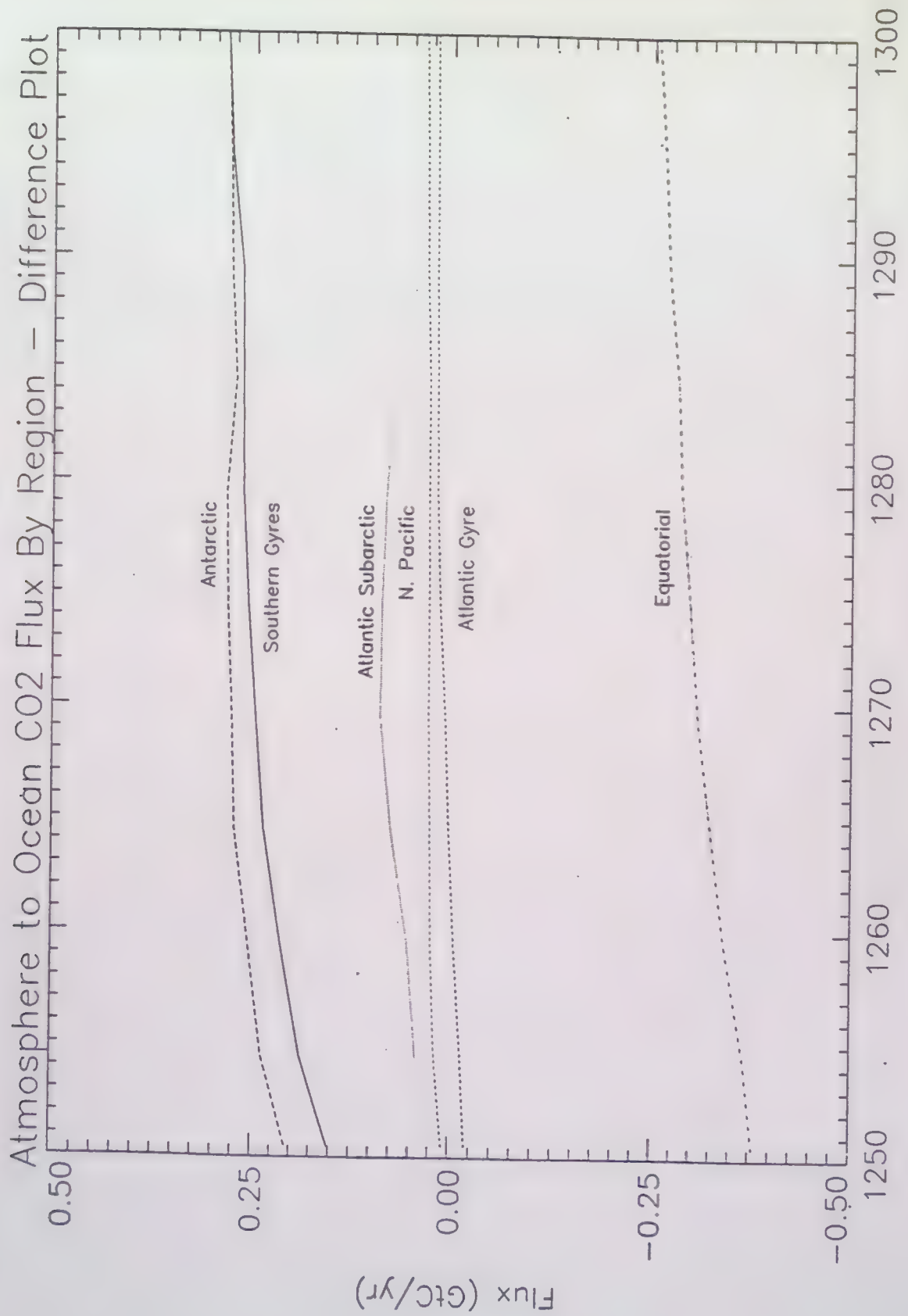

Fig 25 - Time - series of the difference in atmosphere to ocean CO_2 flux for each of the regions defined in Table 3 between experiments B ($\chi_b = 0.5$ cm^2 s^{-1}) and C ($\chi_b = 0.1$ cm^2 s^{-1}).

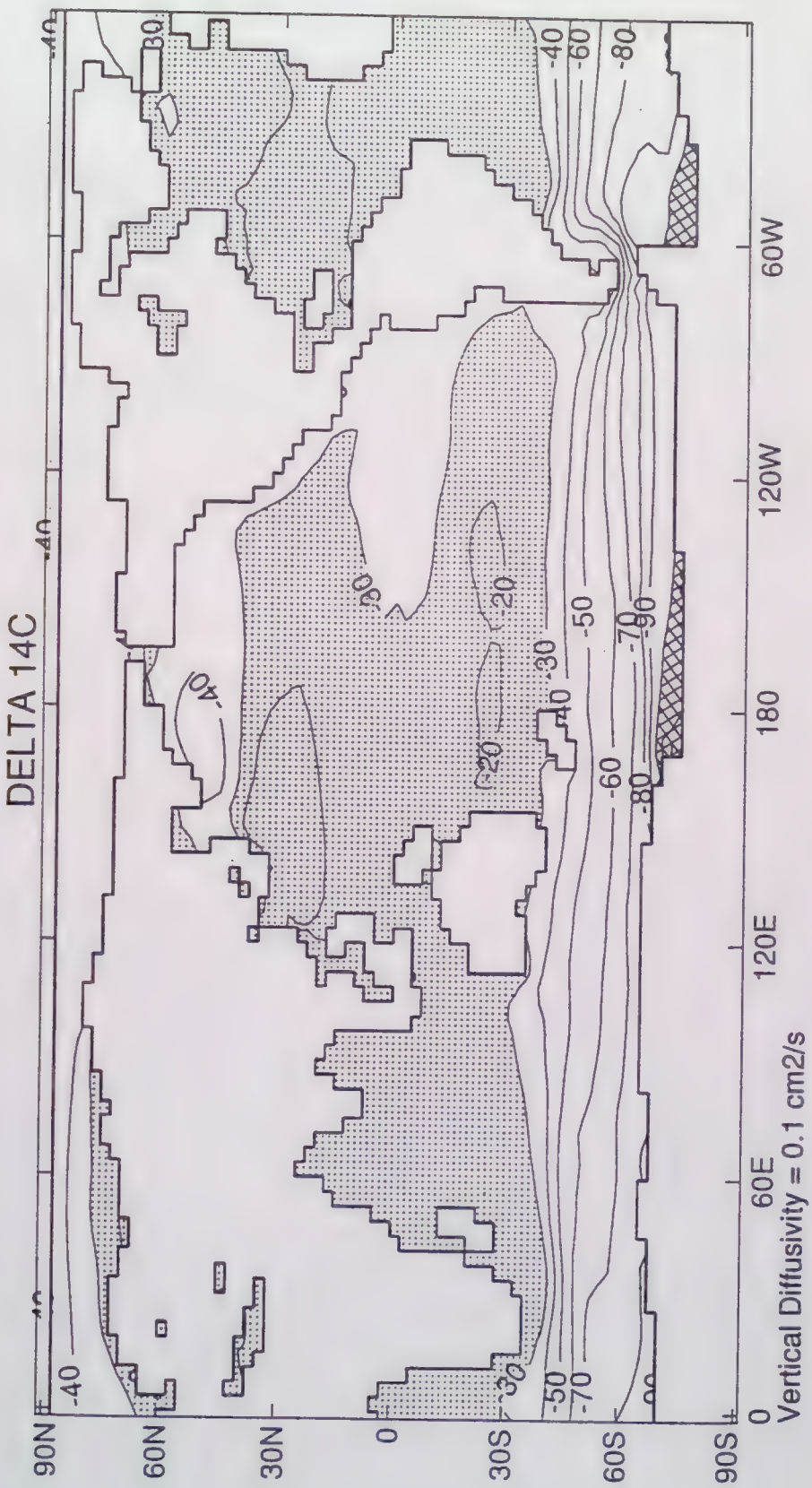

Fig 26 - Predicted $\Delta^{14}C$ (per mil) at the surface from the low diffusivity run of the model. Values ihigher than -30‰ are lightly stippled. Values lower than -100‰ are cross-hatched.

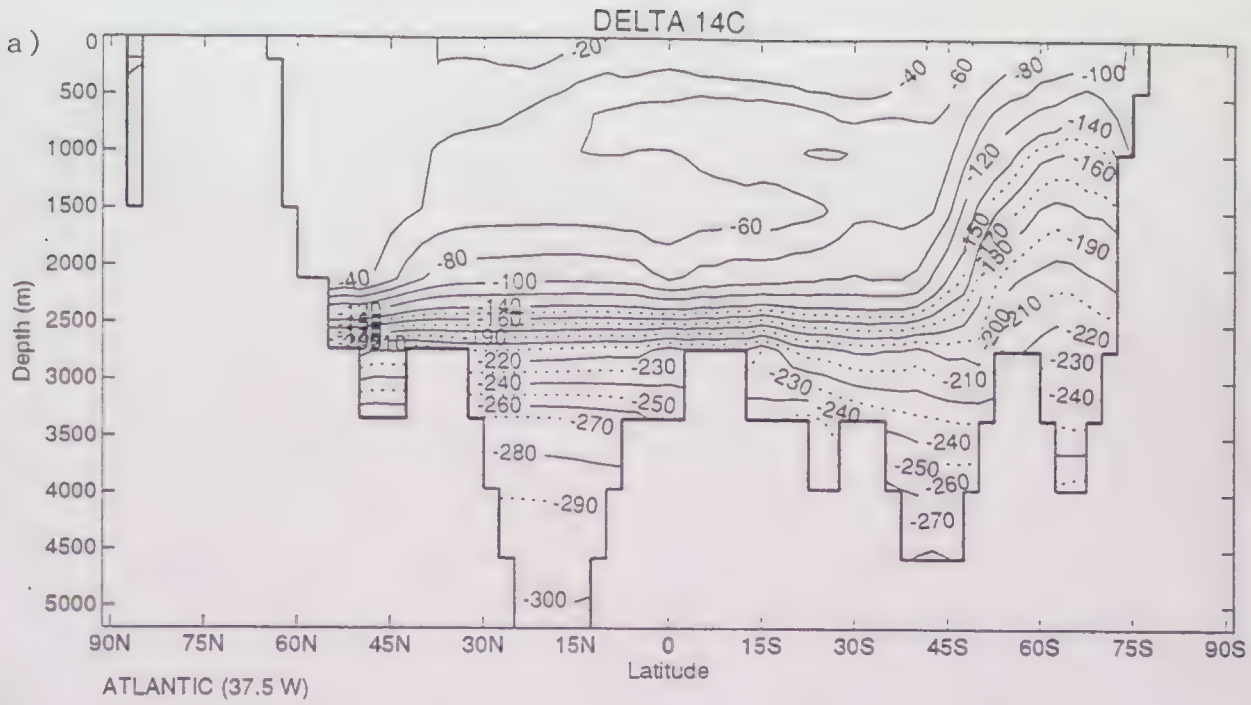

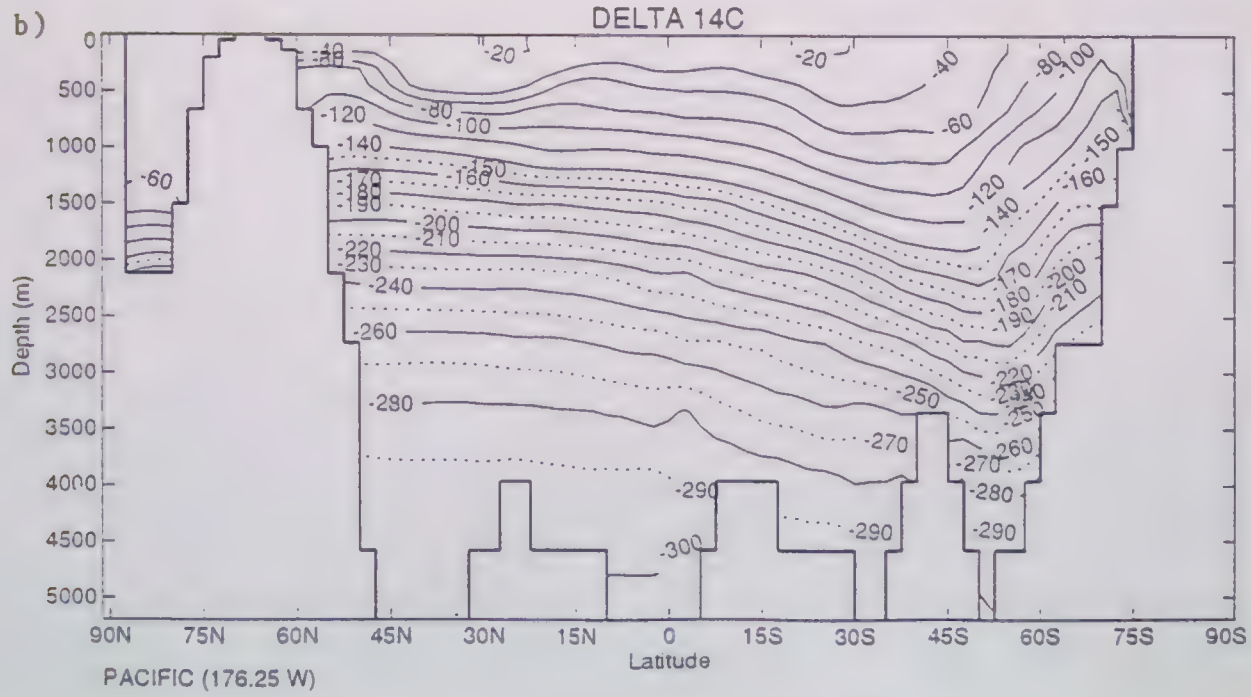

Fig 27 - Predicted latitude-depth cross-sections of $\Delta^{14}C$ (per mil) through a) the Atlantic at 37.5 ^{0}W, and b) the Pacific at 176.25 ^{0}W from the low diffusivity run.

CLIMATE RESEARCH TECHNICAL NOTES

CRTN 1	Oct 1990	Estimates of the sensitivity of climate to vegetation changes using the Penman-Monteith equation. P R Rowntree
CRTN 2	Oct 1990	An ocean general circulation model of the Indian Ocean for hindcasting studies. D J Carrington
CRTN 3	Oct 1990	Simulation of the tropical diurnal cycle in a climate model. D P Rowell
CRTN 4	Oct 1990	Low frequency variability of the oceans. C K Folland, A Colman, D E Parker and A Bevan
CRTN 5	Dec 1990	A comparison of 11-level General Circulation Model Simulations with observations in the East Sahel. K Maskell
CRTN 6	Dec 1990	Climate Change Prediction. J F B Mitchell and Qing-cun Zeng
CRTN 7	Jan 1991	Deforestation of Amazonia - modelling the effects of albedo change. M F Mylne and P R Rowntree
CRTN 8	Jan 1991	The role of observations in climate prediction and research. D J Carson
CRTN 9	Mar 1991	The greenhouse effect and its likely consequences for climate change. D J Carson
CRTN 10	Apr 1991	Use of wind stresses from operational N.W.P. models to force an O.G.C.M. of the Indian Ocean. D J Carrington
CRTN 11	Jun 1991	A new daily Central England Temperature series, 1772-1991. D E Parker, T P Legg and C K Folland
CRTN 12	Jul 1991	Causes and predictability of Sahel rainfall variability. D P Rowell, C K Folland, K Maskell, J A Owen, M N Ward

CLIMATE RESEARCH TECHNICAL NOTES

CRTN 13	Jul 1991	Modelling changes in climate due to enhanced CO2, the role of atmospheric dynamics, cloud and moisture. C A Senior, J F B Mitchell, H Le Treut and Z-X Li
CRTN 14	Sep 1991	Sea temperature bucket models used to correct historical SST data in the Meteorological Office. C K Folland
CRTN 15	Aug 1991	Modelling climate change, and some potential effects on agriculture in the U.K. P R Rowntree, B A Callander and J Cochrane
CRTN 16	Aug 1991	The Boreal Forests and Climate G Thomas and P R Rowntree
CRTN 17	Aug 1991	Development of a Stratosphere-Troposphere Data Assimilation System. R Swinbank.
CRTN 18	Sep 1991	A study of asynchronous coupling using a simple climate model. M K Davey.
CRTN 19	Sep 1991	The Oceanic Carbon Cycle. N K Taylor
CRTN 20	Nov 1991	Worldwide ocean-atmosphere surface fields in Sahel wet and dry years using provisionally corrected surface wind data. M N Ward
CRTN 21	Dec 1991	Coupled tropical ocean global atmosphere models at the UKMO. M K Davey, C Gordon, S Ineson and S Lawrence
CRTN 22	Dec 1991	Empirical parameterisation of tropical ocean-atmosphere coupling. M Allen, M K Davey, D L T Anderson and P D Killworth
CRTN 23	Feb 1992	The temporal evolution of Equatorial Currents in the Indian Ocean D L T Anderson, D J Carrington, R A Corry and C Gordon
CRTN 24	Feb 1992	Stratospheric analyses provided by the U.K. Meteorological Office M J Bailey, A O'Neill and V D Pope

CLIMATE RESEARCH TECHNICAL NOTES

CRTN 25	Feb 1992	Modelling interannual variability in the Indian Ocean using momentum fluxes from the UKMO and ECMWF operational weather analyses. D L T Anderson and D J Carrington
CRTN 26	Mar 1992	A GCM simulation of the impact of Amazonian deforestation on climate using an improved canopy representation J Lean and P R Rowntree
CRTN 27	Mar 1992	The parameterization of rainfall interception in GCMs A J Dolman and D Gregory
CRTN 28	Jun 1992	Development of worldwide marine data eigenvectors since 1985 A W Colman
CRTN 29	Jun 1992	A tropical ocean model with reduced physics M K Davey
CRTN 30	Jun 1992	International Temperature Workshop, Boulder, Colorado, USA, 16 January 1992 Edited by D E Parker
CRTN 31	Jul 1992	Simulation of clear-sky outgoing longwave radiation over the oceans using operational analyses A Slingo and M J Webb
CRTN 32	Sep 1992	A prediction of the transient response of climate J M Murphy
CRTN 33	Nov 1992	LEPS scores for assessing climate model simulations and long-range forecasts. C K Folland
CRTN 34	Jan 1993	Stratospheric Data Assimilation System Guide Editer: R Swinbank
CRTN 35	Mar 1993	A Stratosphere-Troposphere Data Assimilation System R Swinbank and A O'Neill
CRTN 36	Mar 1993	Validation of hydrological schemes for climate models against catchment data. P R Rowntree and J Lean

CLIMATE RESEARCH TECHNICAL NOTES

CRTN 37	Apr 1993	Modelling of palaeoclimates: Examples from the recent past J F B Mitchell
CRTN 38	May 1993	A simulation of seasonality in ENSO forecast skill M K Davey, D L T Anderson and S Lawrence
CRTN 39	Jul 1993	ENSO Prediction experiments using a simple ocean-atmosphere model D-H Wu, D L T Anderson and M K Davey
CRTN 40	Sep 1993	Diagnosis of dynamic sea-surface and sea-level changes from the Cox ocean model J M Gregory
CRTN 41	Sep 1993	Seasonal variations of the clear-sky greenhouse effect: the role of changes in atmospheric temperatures and humidities M J Webb, A Slingo and G L Stephens
CRTN 42	Nov 1993	Sea-level changes under increasing atmospheric CO_2 in a transient coupled ocean-atmosphere GCM experiment. J M Gregory
CRTN 43	Dec 1993	Global and regional patterns of climate change: recent predictions for the Arctic P R Rowntree
CRTN 44	Feb 1994	The effect of changing horizontal diffusion in the atmospheric version of the unified climate model C D Hall and R A Stratton
CRTN 45	Mar 1994	Simulation of El-Niño/Southern Oscillation like variability in a global AOGCM and its response to CO_2 increase. S F B Tett
CRTN 46	Apr 1994	Global data required for monitoring climate change. D E Parker and C K Folland
CRTN 47	May 1994	Seasonal uptake of anthropogenic CO_2 in an ocean general circulation model. N K Taylor